Rodrigues, S., Gonçalves, J., & Terry, J. R. (2007). Existence and stability of limit cycles in a macroscopic neuronal population model.

Early version, also known as pre-print

Existence and stability of limit cycles in a macroscopic neuronal population model.

Serafim Rodrigues[†], Jorge Gonçalves[+] and John R. Terry[†]

(†) Department of Engineering Mathematics, University of Bristol, BS8 1TR, UK

(+) Department of Engineering, University of Cambridge, Trumpington Steet, Cambridge CB2 1P7, UK

June 13, 2007

Abstract

We present rigorous results concerning the existence and stability of limit cycles in a macroscopic model of neuronal activity. The specific model we consider is developed from the Ki set methodology, popularized by Walter Freeman. In particular we focus on a specific reduction of the KII sets, denoted RKII sets. We analyse the unfolding of supercritical Hopf bifurcations via consideration of the normal forms and centre manifold reductions. Subsequently we analyse the global stability of limit cycles on a region of parameter space and this is achieved by applying a new methodology termed *Global Analysis of Piecewise Linear Systems*. The analysis presented may also be used to consider coupled systems of this type. A number of macroscopic mean-field approaches to modelling human EEG may be considered as coupled RKII networks. Hence developing a theoretical understanding of the onset of oscillations in models of this type has important implications in clinical neuroscience, as limit cycle oscillations have been demonstrated to be critical in the onset of certain types of epilepsy.

PACS: 87.10.+e, 87.19.-j, 87.18.-h 05.45.-a

Keywords: human EEG; mathematical modelling; macroscopic population model; normal forms; global stability; limit cycle oscillations; epilepsy

1 Introduction

We consider a population model that represents the aggregate activity of an ensemble of neurons within a neural region, for example a cortical column containing interacting inhibitory and excitatory neurons.

The type of model that we consider was discussed by Freeman [1, 2], where they were used to model a series of experimental observations, and are denoted the Ki set hierarchy, where $i = \{0, I, II, III\}$. At each level of the hierarchy the complexity of the topology increases and the type of connections allowed between excitatory and inhibitory are well specified. The K0 set is the most basic and simplest component in the hierarchy consisting of three parts, resembling biologically a real neuron. Specifically, K0 sets model a neuronal ensemble forming part of a cortical column within which all neurons share the same physiological and functional properties. They receive spatial inputs (dendrites) which are weighted and summed. Further they include a soma where spikes are produced, however the internal dynamics (the transmembrane potential of a neuron) follows a linear time invariant system with second order dynamics, meaning that the voltage response of each population in the model has finite rise and decay times. This is in contrast to other firing-rate models such as that introduced by Wilson and Cowan [3] in which voltages are represented by a first order differential equation. The output is then shaped by a nonlinear saturating function, that essentially provides a measure of the relationship between the transmembrane potential and an averaged neuronal firing rate.

On the next level of the hierarchy, a KI set is formed by two K0 sets and defines the coupling relationship between them. However, this structure allows populations to be only either exclusively excitatory or inhibitory and no auto-feedback is allowed. Subsequently, a KII set consists of two KI sets (or four KO sets). KII networks can function as an encoder of signals or as an auto-associative memory [1, 4]. Mathematically, KII sets may have several fixed points and can also have limit cycle attractors depending on the parameters of the system and the initial conditions. At the final level of the hierarchy is the KIII set. These KIII networks may have different layers of KII sets representing for example different anatomical regions of the mammalian brain. As an example, a computational KIII network designed to model the olfactory system has been studied by Heng-Jen et al. [5]. The KIII network may have strange attractors and positive Lyapunov exponents, consequently exhibiting chaotic oscillations [4, 6]. A complete understanding of the total hierarchy would represent the knowledge to mimic and predict EEG signals and thus comprehend brain functioning at the macroscopic level [2].

Much of Freeman's work presents extensive studies of KII and KIII networks from a signal processing perspective and consequently an understanding of network dynamics is still incomplete. The complexity of these sets is such that analytical results are scarce and a full analysis of KIII networks is beyond current techniques. However, some interesting results towards this goal have been presented in [7], where analysis is made possible by considering a non-symmetric sigmoid function with derivative equal to one at the equilibrium point, thus simplifying the overall analysis. A further interesting study by Xu

and Principe [8] also employs a non-symmetric sigmoid, but considers a subset of the KII set, denoted RKII models. These are a simplification of a KII set consisting of two KI-type sets but each containing two different neurons, excitatory and inhibitory, (note that KI sets have either excitatory or inhibitory but not both). Further, an RKII set does not have recurrent coupling within a population. This work motivates the present study with the objective to understand RKII sets without the restriction of a non-symmetric sigmoidal function.

It is important to recognise the fundamental differences between a model determined via observations of the neural-mass and those developed by considering populations of individual neurons, where the dynamics of each individual neuron is described by biophysical models [9]. In the latter case, physiological quantities such as ionic currents can be determined from experiments and incorporated directly, whereas in the former case these appear only in an average sense. Not only this, but in the case of biophysical models, these currents determine the complex behaviour, i.e. firing-rate patterns. Whereas, in the case of neural-mass or lumped models [10] it is the interactions between the populations that give rise to complex dynamics, that may be observed at macroscopic scales (e.g. EEG). Interestingly despite these approaches being at opposite extremes, both have been shown to replicate experimentally recording dynamics. For example, in the work presented in [11, 12], a macroscopic model derived from Freeman mass-action approach was shown to mimic the transitions observed in clinically recorded data from subjects with petit-mal seizures. In particular, the transition from healthy dynamics to seizures was heralded by the occurrence of a limit-cycle oscillation in the recorded EEG. An RKII set with two hierarchical levels would give us the ability to understand transitions of this type. Results for RKII networks with three hierarchical levels would offer insight into studies related to connections of three areas of the brain, for example interactions of cortical, thalamic and basal ganglia (striatum) and could shed light on the understanding of complex partial seizures [13]. Our previous work [12] gave some analytical insight to the nature of spike-wave morphology observed in generalised seizures, but to further develop analytical results and consequently understand the full dynamical properties of an RKII network (or even higher level networks) it is necessary to pursue another direction of study.

Confining ourselves to a single RKII set is a first step towards a future understanding of interactions between multiple regions. Thus, the purpose of the present work is to identify and analyse limit cycles generated in an RKII set and possibly refine or map the dynamic equation for each population to the microscale (i.e. biophysical models), so as to better describe the mechanisms of oscillations arising from an ensemble of neurons. In fact, we have conducted a preliminary work that demonstrates under certain assumptions how to map these equations onto a reduced conductance-based model [14]. This contrasts

with first-order neural field models, such as those of Wilson and Cowan [3], where the activity of a neuronal population is represented by a single-state variable. This describes the proportion of neurons becoming active per unit time. The rise time of the population is assumed to occur infinitely quickly with only a finite delay, so that the firing rate of the action potentials of the neuronal population is governed by a first order differential equation. Such models may be derived directly from Hodgkin-Hoxley type formulations.

The focus of our present work is on the existence and stability of limit cycles in neural-mass models. We achieve this by developing a linear stability theory and contrast this with numerical continuation results obtained using XPPAUT [15]. We then consider analytically the unfolding of the bifurcations by using normal forms to give sufficient conditions for the existence of limit cycles and to study global stability of these oscillations. Global stability is in general a difficult problem to address. It is typically only in special cases that it is possible to find, for example, Lyapunov functions guaranteeing global stability of fixed points and even more harder to prove global stability of limit cycles. To understand the global properties of the limit cycles of the RKII set we consider a piecewise linear version of the system and prove global stability for a restricted region of the parameter space. To this end, we use a recent formalism termed, *Global Analysis of Piecewise Linear Systems* [16].

2 Description of the model

The specific choice of the model equations we consider arise out of the thalamic modules of a neural mass model used to study human EEG [11]. The model is a reduction of a cortico-thalamic model by Robinson et al. [17, 18], which is essentially derived from the work of Freeman [1], Lopes da Silva [19] and incorporates a wave-like equation for propagation of cortical activity developed by Jirsa and Haken [20]. Parameters of the model were chosen to lie within physiological estimates, as described in [18]. A schematic of the model is shown in Fig. 1(a), which represents an ensemble of interacting inhibitory and excitatory neurons and is defined in the following way:

$$\begin{cases} \frac{d^2}{dt^2}V_s(t) + (\alpha+\beta)\frac{d}{dt}V_s(t) + \alpha\beta V_s(t) = \alpha\beta(\nu_{sr}\varsigma[V_r(t)] + \nu_{sn}\phi_n) \\ \frac{d^2}{dt^2}V_r(t) + (\alpha+\beta)\frac{d}{dt}V_r(t) + \alpha\beta V_r(t) = \alpha\beta\nu_{rs}\varsigma[V_s(t)] \end{cases} \tag{1}$$

where $\nu_{sr} \in \mathbb{R}^-$, $\nu_{rs} \in \mathbb{R}^+$, $\nu_{sn} \in \mathbb{R}_0^+$ and

$$\varsigma[V_a(t)] = \frac{Q_a^{\max}}{1 + \exp\left(-\frac{\pi}{\sqrt{(3)}}\frac{V_a(t)-\theta_a}{\sigma_a})\right)}$$

is a unipolar sigmoidal function illustrated in Fig. 1(b) that represents the relationship between the transmembrane potential V_a (commonly expressed as *wave amplitude*) and the axonal firing rate $\varsigma(V_a)$ (which is often referred to as the *pulse density*). Without loss of generality, in the language of the work of Robinson and others, $a = \{r, s\}$ refers to the reticular nuclei (an inhibitory neuronal population) and the specific relay nuclei (an excitatory neuronal population) respectively. However these could represent any excitatory and inhibitory neuronal ensembles. The variable V_a represents averaged post-synaptic dendritic potentials as would be evaluated by extracellular measurements of EEGs. Here, the second order equations model a relationship between the induced transmembrane voltage $V_a(t)$ and the incoming dendritic impulses. The parameters α and β are constants representing the inverse rise and decay times parameterising the response to these impulses. The conversion of pulse density $\varsigma(V_a)$ to a wave amplitude is implicit in the synaptic weights ν_{sr} and ν_{rs}. Note that these synaptic weights can not be measured directly, either experimentally or by other means, and consequently can only be inferred indirectly through the modeling process, i.e. it is an indirect measure of the synaptic transmission. The neuronal ensembles can be driven by an external signal, for example noise ϕ_n, but here we restrict ourselves to a constant time invariant signal (which can be either off or on), future work will also consider periodic signals to complement our results obtained in [12]. The relevant parameters values of the given model are provided in Table 1.

3 Stability analysis

In this section we provide an overview of the results concerning linear stability analysis. We perform a bifurcation analysis of the model, examining the possible types of dynamics of the thalamic RKII set. We also demonstrate necessary conditions on the parameters of the model for stability of a limit cycle oscillation.

Using appropriate substitutions, we re-write system (1) as four coupled first order ODEs:

$$\begin{cases} \frac{d}{dt}V_s(t) &= w(t), \\ \frac{d}{dt}w(t) &= -\alpha\beta V_s(t) - (\alpha+\beta)w(t) + \alpha\beta(\nu_{sr}\varsigma[V_r(t)] + \nu_{sn}\phi_n) \\ \frac{d}{dt}V_r(t) &= v(t), \\ \frac{d}{dt}v(t) &= -\alpha\beta V_r(t) - (\alpha+\beta)v(t) + \alpha\beta\nu_{rs}\varsigma[V_s(t)]. \end{cases} \tag{2}$$

The stability of the equilibrium points of this first order system may be be analysed by ensuring that the linearised version of (2) satisfies the Hartman-Groβman theorem [21]. Consequently, we consider

the Jacobian matrix of (2):

$$\mathbf{J} = \begin{pmatrix} 0 & 1 & 0 & 0 \\ -\alpha\beta & -(\alpha+\beta) & \alpha\beta\nu_{sr}\varsigma'[V_r^\star] & 0 \\ 0 & 0 & 0 & 1 \\ \alpha\beta\nu_{rs}\varsigma'[V_s^\star] & 0 & -\alpha\beta & -(\alpha+\beta) \end{pmatrix}, \tag{3}$$

where V_s^* and V_r^* are the values of V_s and V_r at some equilibrium point and $\varsigma'[V_a] = \frac{d}{dV_a}\varsigma(V_a)$ (i.e. the derivative of $\varsigma(V_a)$ with respect to the transmembrane potential). The equilibrium state being determined by setting the RHS of system (2) equal to 0, thus giving:

$$\begin{cases} V_s = \nu_{sr}\varsigma[V_r] + \nu_{sn}\phi_n, \\ V_r = \nu_{rs}\varsigma[V_s], \end{cases} \tag{4}$$

the eigenvalues of which are given by the roots of the characteristic equation:

$$\lambda = \frac{-(\alpha+\beta) \pm \sqrt{(\alpha-\beta)^2 \pm 4i\alpha\beta\sqrt{|\nu_{sr}\nu_{rs}|\varsigma'[V_r^\star]\varsigma'[V_s^\star]}}}{2}. \tag{5}$$

It is apparent that there exist two complex conjugate pairs of eigenvalues, with one pair trailing the other (by which it is meant the real part is less). Furthermore, the real part of the eigenvalues is defined as

$$\mathbf{Re}(\lambda) = \frac{1}{2}\left[-(\alpha+\beta) \pm \frac{\sqrt{2}}{2}\sqrt{\sqrt{(\alpha-\beta)^4 + (4\alpha\beta)^2|\nu_{sr}\nu_{rs}|\varsigma'[V_r^\star]\varsigma'[V_s^\star]} + (\alpha-\beta)^2}\right].$$

A Hopf bifurcation will occur when $\mathbf{Re}(\lambda) = 0$. The form of this expression makes verifying this condition difficult and a more convenient treatment is to use the Lienard-Chipart criterion (derived from the more familiar Routh-Hurwitz Theorem) [22]. Using this criterion we derived in [12] the same result obtained by Xu and Principe [8], obtaining the following hyperbolic curve in the $|\nu_{sr}\nu_{rs}|$ parameter space:

$$|\nu_{sr}\nu_{rs}| > \frac{1}{\varsigma'[V_r^*]\varsigma'[V_s^*]}\frac{(\alpha+\beta)^2}{\alpha\beta} \tag{6}$$

A graphical representation of which is shown in Fig. 2(a). It is important to note that the right hand side of (6) is also a function of ν_{sr} and ν_{rs}, implying a nonlinear dependence on $|\nu_{sr}\nu_{rs}|$. If condition (6) is satisfied then the equilibrium has a transition from a stable to unstable equilibrium state, via an apparent supercritical Hopf bifurcation. This may be proven analytically by considering the normal forms of (2) which we develop in section 4, or by evaluating the coefficients of curvature [23, 24].

In the following discussion we analyse system (2) for the autonomous case, as the case when the system is driven by a time invariant signal, may be considered as a transformation of the coordinate system, describing the transition to instability in each scenario. The nullclines of the system may be calculated from (4) and an illustrative example is presented in Fig. 2(b). We observe that the system has a unique equilibrium state since $\varsigma(V)$ is a monotone increasing function. Furthermore, the equilibrium state can be either in the first or the fourth quadrant of the state space (V_r, Vs), depending on the strength of the external input ν_{sn}. Detailed discussion of the results concerning the bifurcations of the system when driven by an external signal will be published elsewhere.

As discussed previously, in the autonomous case the equilibrium is in the fourth quadrant of the state space (V_r, V_s). Further, from Xu and Principe [8] we have the following properties of the equilibrium state:

i) V_s^* is a decreasing function with respect to both ν_{rs} and $|\nu_{sr}|$, that is, $\frac{dV_s^*}{d\nu_{rs}} \leq 0$ and $\frac{dV_s^*}{d|\nu_{sr}|} \leq 0$

ii) V_r^* is an increasing function with respect to ν_{rs} but decreasing with respect to $|\nu_{sr}|$, i.e, $\frac{dV_r^*}{d\nu_{rs}} \geq 0$ and $\frac{dV_r^*}{d|\nu_{sr}|} \leq 0$

From these properties, we may define a local region (since finding a global region is analytically intractable) for which the stability condition (6) is satisfied and hence gives rise to a transition between a stable equilibria and a stable limit cycle. For condition (6) to hold true it is necessary that if $|\nu_{sr}\nu_{rs}|$ increases then $1/(\varsigma^{'}[V_r^*]\varsigma^{'}[V_s^*])$ should decrease to a minimum in order to satisfy the inequality. In other words, $\varsigma^{'}[V_r^*]\varsigma^{'}[V_s^*]$ should be maximized. One way to define the region is by noticing that the equilibrium is in the fourth quadrant and by tuning the parameters ν_{rs} and ν_{sr} according to Properties (i) and (ii) it is possible to find a lower and upper bound for $V_s^\star$ and $V_r^\star$. For instance, if we have that both $V_s < \theta$ and $V_r < \theta$ then the only form to maximise $\varsigma^{'}[V_r^*]\varsigma^{'}[V_s^*]$ is to first fix $\nu_{sr} = \nu_{sr}^\star$ and then increase ν_{rs} until condition (6) is satisfied. Note that increasing ν_{rs} decreases $V_s^\star$. A similar stability curve was obtained by Ilin and Kozma in [**?**], whom considered both an RKII set and a KII set. The case of a KII set merely resulted in a shifting of the hyperbolic curve in the total parameter space.

3.1 Numerical continuation

We further investigated the behaviour of the RKII model numerically using the software package XPPAut [15], both to examine the many interesting dynamical features of the model and also to verify the analytical findings. Consequently, our first investigation was to examine the (ν_{sr}, ν_{rs}) parameter space

and compare these results with our analytical finding (6). Here, an unexpected result was to observe that the stability curve in (ν_{sr}, ν_{rs}) parameter space was more far reaching than that expressed by condition (6). In addition to the hyperbolic curve described by condition (6), there was also a fold point on the same branch in parameter space. To obtain this branch numerically, we first found a Hopf bifurcation point and we then perform a two parameter continuation, depicted in Fig. 3.

The notation used is the same as the software package XPP to denote special points, i.e *Supercritical Hopf* (HB) and *Fold or Limit point* (LP). Starting at any point on the (ν_{sr}, ν_{rs}) curve, for example HB1, and then by varying only ν_{rs}, we observe in the bifurcation diagram (V_a, ν_{rs}) that the system will have periodic orbits with increasing amplitude. This amplitude however decreases when the parameter ν_{rs} increases. An example of such a scenario is depicted in Fig. 4(a). Conversely, if we start at HB1 and vary the parameter ν_{sr} by increasing it, we find the upper branch of the (ν_{rs}, ν_{sr}) curve emanating from the fold LP1. Thus, the resulting diagram will have periodic orbits that have an increasing and subsequently decreasing amplitude until convergence at a second Hopf point. This latter idea is illustrated in Fig. 4(b). The values for HB1, HB2 and LP are provided in Table 2.

The existence of a fold point in the (ν_{sr}, ν_{rs}) parameter space suggests that the parametric curve depicted in Fig. 3 is globally parabolic with the vertex given by the fold point (LP1) and locally hyperbolic as described by condition (6). The difference between these two curves (Fig. 2 and Fig. 3) is because to plot (6) we had to fix $V_s^\star$ and $V_r^\star$ so it is only a local representation.

4 Normal form calculation for an RKII set

In the previous sections we investigated the linearised flow of the RKII model and defined necessary conditions for local stability. In this situation varying the control parameters of the model will not change the structural stability of the system. However, in our numerical study we found that for some parameter regimes the RKII set exhibits a limit cycle, i.e. a structural change in the flow. The change or bifurcation in general occurs where linear stability yields an instability, that is, through the implicit function theorem the solution cannot be continued smoothly because the Jacobian becomes singular. In general, when the eigenvalues have zero real part the question on how to relate the flow of the linear version of a system with its nonlinear counterpart is non-trivial. Fortunately, in this case, one can address whether the nonlinear system posses a manifold having similar properties to the linear space spanned by the centre eigenspace and this can be answered by using the centre manifold theory. We proceed by calculating the centre manifold of this system. Furthermore, through linear stability analysis

only necessary conditions for the appearance of a supercritical Hopf bifurcation were made possible. However, according to [23, 24] it is also necessary to demonstrate that the curvature coefficient ([24], Eq. (6.1.4)) is nonzero, which provides a sufficient condition for the Hopf bifurcation to occur. The sign of the curvature determines the local stability and if positive (negative) indicates it is a supercritical (subcritical) bifurcation. In general, the expansion of the curvature coefficient becomes complicated for high dimensional systems.

Alternatively, calculation of the normal forms allows studying the vector field locally in some neighbourhood. This is achieved through an iterative procedure, either simplifying or identifying the nonlinear terms from the Taylor approximation of the vector field that correspond to the observed dynamics. From this method we can determine the minimal set of equations describing the flow and indirectly providing the specific coefficients for the Hopf bifurcation. Once the reduced set of equations has been determined then, for example, an option of study is to consider the coupling of the reduced nonlinear equations and look for dynamical features observed in the full system of (i.e. without normal forms) coupled RKII sets. In the present study we lay the foundations for this future work, by presenting these calculations in the thalamic subsystem case.

To perform this calculation, we follow the methodology of Iooss and Adelmeyer [25] which allows calculation of the normal forms, as well as the centre manifold reduction in one unique step. This technique was initially proposed by Elphick [26], where it was shown that it is always possible to find a near identity coordinate transformation that maps the centre space to the hyperbolic space and one can then incorporate this transformation directly into the normal form. This methodology differs from other techniques in that it does not expand the vector field directly. Instead, it assumes that the structure of the reduced vector field on the centre manifold is known. The Ansatz of the reduced vector field and the near identity transformation are inserted into the Homological operator and from this form the coefficients for the centre manifold of the reduced vector field may be evaluated. This permits minimal computational steps, when compared for example to the Birkhoff normal form transformations considered in [27].

4.1 Notation

The k^{th} order multivariate Taylor series expansion for $P \in C^k(\mathbb{R}^n \times \mathbb{R}^m; \mathbb{R}^n)$ may be represented concisely using the following formula:

$$P(z,\nu) = \sum_{\substack{\psi\in\Gamma^n \\ \chi\in\Lambda^m}} P^{|\chi|}_{|\psi|}[z^\psi, \nu^\chi] + \mathcal{O}(|z|^{|\psi|} + |\nu|^{|\chi|}), \tag{7}$$

where $z \in \mathbb{R}^n$, and $\nu \in \mathbb{R}^m$ is the set of parameters. The multi-index sets are defined by

$$\begin{aligned} \Gamma^n &= \{(\psi_1, \psi_2, \cdots, \psi_n) | \psi_i \in \{0,1,2,\cdots\}\}, \\ \Lambda^n &= \{(\chi_1, \chi_2, \cdots, \chi_n) | \chi_i \in \{0,1,2,\cdots\}\}, \end{aligned} \tag{8}$$

where the order of the polynomial is defined by the order of the multi-index $|\psi| = \psi_1 + \psi_2 + \cdots \psi_n$ and $|\chi| = \chi_1 + \chi_2 + \cdots \chi_n = k$. $P_{|\psi|}[z^\psi, \nu^\chi]$ is a $|\psi|$-linear map on z and $|\chi|$-linear map on the parameters, where $z^\psi = z_1^{\psi_1} \cdots z_n^{\psi_n}$ and $\nu^\psi = \nu_1^{\chi_1} \cdots \nu_m^{\chi_m}$. In coordinates, the i-th component is defined as follows

$$(P^{|\chi|}_{|\psi|}(z^\psi, \nu^\chi))_i = \sum_{|\psi|+|\chi|=k} (p^\chi_\psi z^\psi \nu^\chi)_i \tag{9}$$

where p^χ_ψ represents the polynomial coefficients expressed by

$$p^\chi_\psi = \frac{1}{(\psi_1! \cdots \psi_n!)(\chi_1! \cdots \chi_m!)} \left[\left(\frac{\partial}{\partial z_1}\right)^{\psi_1} \cdots \left(\frac{\partial}{\partial z_n}\right)^{\psi_n} \left(\frac{\partial}{\partial \nu_1}\right)^{\chi_1} \cdots \left(\frac{\partial}{\partial \nu_m}\right)^{\chi_m} \right]_{|(x,\nu)=(0,0)}$$

The above representations gives a clearer illustration of the k-linear map property of the Taylor expansion. This provides a more abstract means for using the Taylor expansion to derive the normal forms.

4.2 Setup and Statement

Consider the RKII model (1) in the following form

$$\dot{x} = F(x,\nu) \quad x \in \mathbb{R}^4, \nu \in \mathbb{R}^2, \tag{10}$$

where $x = (V_s, w, V_r, v)$. $\nu = (\nu_{sr}, \nu_{rs})$ are the only parameters we allow to vary and the vector field $F \in C^k(\mathbb{R}^4, \mathbb{R}^2)$ for large enough k. To simplify the complexity of the calculation, we may rewrite system (1) by first considering a linear change of variables that shifts the Hopf bifurcation, say (x^*, ν^*), to zero and then expand the vector field around $(\widehat{x}, \widehat{\nu}) = (0,0)$. Setting the linear change of variables to $\widehat{x} = x - x^*$ and $\widehat{\nu} = \nu - \nu^*$ and substituting appropriately into equations (1) we obtain the following

$$\dot{\widehat{x}} = F(\widehat{x}, \widehat{\nu}) \tag{11}$$

where now $F(0,0)=0$, and further by expanding the vector field with respect to $\widehat{x}$ we determine:

$$\dot{\widehat{x}} = J(\widehat{x}) + N(\widehat{x}), \quad N = \mathcal{O}(|\widehat{x}|(\widehat{x},\widehat{\nu})), \tag{12}$$

where J is the Jacobian (3) and N denotes the nonlinear terms. Specifically for the Hopf bifurcation we expect to have in the Taylor expansion, terms that depend both linearly on the coordinates and also on the control parameters, where these terms result in the following

$$N_1^{1,0}(\widehat{x}) = \begin{pmatrix} 0 \\ \alpha\beta\frac{\partial\varsigma[V_r^\star]}{\partial\widehat{V_r}}\hat{\nu_{sr}}\widehat{V_r} \\ 0 \\ 0 \end{pmatrix} \quad , \quad N_1^{0,1}(\widehat{x}) = \begin{pmatrix} 0 \\ 0 \\ 0 \\ \alpha\beta\frac{\partial\varsigma[V_s^\star]}{\partial\widehat{V_s}}\widehat{V}_s\hat{\nu_{rs}} \end{pmatrix}.$$

The subscript (1) indicates derivative with respect to $\hat{x}$ and the superscript $(1,0)$ and $(0,1)$ denotes derivative with respect to $\hat{\nu_{sr}}$ and $\hat{\nu_{rs}}$ respectively. Equally, the expansion of N should have terms that are cubic in the coordinate space, but independent of the parameters. Thus we have the subsequent expansions

$$N_2^0(\widehat{x_1},\widehat{x_2}) = \frac{1}{2!}\begin{pmatrix} 0 \\ \alpha\beta\nu_{sr}^*\frac{\partial^2\varsigma[V_r^\star]}{\partial\widehat{V_r}^2}\widehat{V_{r,1}}\widehat{V_{r,2}} \\ 0 \\ \alpha\beta\nu_{rs}^*\frac{\partial^2\varsigma[V_s^\star]}{\partial\widehat{V_s}^2}\widehat{V_{s,1}}\widehat{V_{s,2}} \end{pmatrix} \quad , \quad N_3^0(\widehat{x_1},\widehat{x_2},\widehat{x_3}) = \frac{1}{3!}\begin{pmatrix} 0 \\ \alpha\beta\nu_{sr}^*\frac{\partial^3\varsigma[V_r^\star]}{\partial\widehat{V_r}^3}\widehat{V_{r,1}}\widehat{V_{r,2}}\widehat{V_{r,3}} \\ 0 \\ \alpha\beta\nu_{rs}^*\frac{\partial^3\varsigma[V_s^\star]}{\partial\widehat{V_s}^3}\widehat{V_{s,1}}\widehat{V_{s,2}}\widehat{V_{s,3}} \end{pmatrix}$$

where N_3^0 is the third order expansion with respect to $\widehat{x}$ and the superscript zero indicates no dependence on the parameters $\widehat{\nu}$. The computation of the coefficients of the cubic terms N_0^3 depends indirectly on the quadratic coefficients N_0^2 shown above. At a Hopf bifurcation, condition (6) becomes an equality and substituting this into (5), we can determine the following four eigenvalues

$$\begin{cases} \lambda_{1,2} = \pm i\sqrt{\alpha\beta} \\ \lambda_{3,4} = -(\alpha+\beta) \pm i\sqrt{\alpha\beta} \end{cases}, \tag{13}$$

and the associated eigenvectors can be evaluated for one of the conjugate pairs, obtaining:

$$E_{i\sqrt{\alpha\beta}} = \left\{ \begin{bmatrix} \frac{-\nu_{sr}^*\frac{\partial\varsigma[V_r^\star]}{\partial\widehat{V_r}}}{(\alpha+\beta)}\widehat{v} \\ \frac{-\nu_{sr}^*\frac{\partial\varsigma[V_r^\star]}{\partial\widehat{V_r}}i\sqrt{\alpha\beta}}{(\alpha+\beta)}\widehat{v} \\ \frac{-i\sqrt{\alpha\beta}}{\alpha\beta}\widehat{v} \\ \widehat{v} \end{bmatrix} : \widehat{v}\in\mathbb{C} \right\} = Span \left\{ \begin{bmatrix} -\nu_{sr}^*\frac{\partial\varsigma[V_r^\star]}{\partial\widehat{V_r}}\alpha\beta \\ -\nu_{sr}^*\frac{\partial\varsigma[V_r^\star]}{\partial\widehat{V_r}}i\sqrt{\alpha\beta}\alpha\beta \\ -i\sqrt{\alpha\beta}(\alpha+\beta) \\ (\alpha+\beta)\alpha\beta \end{bmatrix} \right\} \tag{14}$$

$$E_{-(\alpha+\beta)+i\sqrt{\alpha\beta}} = \left\{ \begin{bmatrix} \frac{\nu_{sr}^* \frac{\partial \varsigma[V_r^\star]}{\partial \widehat{V_r}}(1-i(\alpha+\beta)\sqrt{\alpha\beta})}{(\alpha+\beta)((\alpha+\beta)^2+\alpha\beta)}\widehat{v} \\ \frac{i\sqrt{\alpha\beta}\nu_{sr}^* \frac{\partial \varsigma[V_r^\star]}{\partial \widehat{V_r}}}{(\alpha+\beta)}\widehat{v} \\ \frac{-(\alpha+\beta)-i\sqrt{\alpha\beta}}{(\alpha+\beta)^2+\alpha\beta}\widehat{v} \\ \widehat{v} \end{bmatrix} : \widehat{v} \in \mathbb{C} \right\}$$

$$= Span \left\{ \begin{bmatrix} \nu_{sr}^* \frac{\partial \varsigma[V_r^\star]}{\partial \widehat{V_r}}(1 - i(\alpha+\beta)\sqrt{\alpha\beta}) \\ i\sqrt{\alpha\beta}\nu_{sr}^* \frac{\partial \varsigma[V_r^\star]}{\partial \widehat{V_r}}((\alpha+\beta)^2 + \alpha\beta) \\ -((\alpha+\beta) + i\sqrt{\alpha\beta})(\alpha+\beta) \\ (\alpha+\beta)((\alpha+\beta)^2 + \alpha\beta) \end{bmatrix} \right\} \tag{15}$$

The linearly invariant centre space is spanned by $E_{i\sqrt{\alpha\beta}}$ and its corresponding conjugate eigenvector (i.e a two dimensional manifold) which we denote by $E_0 = span\{e_0, \bar{e_0}\}$ and the linearly invariant hyperbolic space spanned by the remaining two eigenvectors, we denote by $E_h = span\{e_h, \bar{e_h}\}$. Note also that $\mathbb{R}^4 = E_h \oplus E_0$. According to the centre manifold and normal form arguments [25], there exists a neighbourhood $I \in \mathbb{R}^2$ around 0 and a neighbourhood $U \in \mathbb{R}^4$ around 0 and a smooth map $h \in C^k(E_0 \times \mathbb{R}^2; E_h)$ with the following properties:

1. $h(0,0) = 0$ and $D_z h(0,0) = 0$ for $z \in E_0$
2. For $\hat{\nu} \in I$, the manifolds $M_0(\hat{\nu}) = \{(z, h(z,\hat{\nu}))|z \in E_0\}$ are locally invariant to system (11) and contain all solutions of the RKII set near to $\widehat{x} = 0$, $\forall\, t \in \mathbb{R}$ and the map satisfies $D_z h(z,\hat{\nu})\dot{z} = \dot{y}$, where $z \in E_0$ and $y \in E_h$.
3. According to the normal form theory [25] it is possible to determine a polynomial $G \in C^k(E_0 \times \mathbb{R}^2; E_h)$, with $G(0,0) = 0$, $D_z G(0,0) = 0$ such that by a near identity coordinate transformation $\widehat{x} = z + h(z,\hat{\nu})$, $z \in E_0$ the system (12) may be normalized to:

$$\dot{z} = Jz + G(z,\hat{\nu}), \quad G = \mathcal{O}(|z||(z,\hat{\nu})|). \tag{16}$$

In this particular instance, using the assumption that the flow on the centre manifold is locally periodic, the presence of the Hopf bifurcation implies that equation (16) has a known form. In particular the Jacobian, J of system (1) on the centre manifold has simple eigenvalues $\pm i\sqrt{\alpha\beta}$. Using complex notation we can express the centre manifold in the following way

$$E_0 = \{z = Ze_0 + \bar{Z}\bar{e_0} \quad |Z \in \mathbb{C}\} \tag{17}$$

Where Z and $\bar{Z}$ are the coordinates on the manifold and it follows that the normalized flow is given by

$$\begin{cases} \dot{Z} = i\sqrt{\alpha\beta}Z + ZQ(|Z|^2, \hat{\nu_{sr}}, \hat{\nu_{rs}}) + \mathcal{O}(|Z|^{2k+3}) \\ \dot{\bar{Z}} = -i\sqrt{\alpha\beta}\bar{Z} + \bar{Z}\bar{Q}(|Z|^2, \hat{\nu_{sr}}, \hat{\nu_{rs}}) + \mathcal{O}(|Z|^{2k+3}) \end{cases}, \tag{18}$$

where $Q(|Z|^2, \hat{\nu_{sr}}, \hat{\nu_{rs}})$ is a complex polynomial of degree k in $|Z|^2$ with $Q(0,0) = 0$ that depends smoothly on the control parameters $(\hat{\nu_{sr}}, \hat{\nu_{rs}})$. In particular, by expanding $ZQ(|Z|^2, \hat{\nu_{sr}}, \hat{\nu_{rs}})$ using (7) we obtain:

$$ZQ(|Z|^2, \hat{\nu_{sr}}, \hat{\nu_{rs}}) = g_{1,0}^{1,0}\hat{\nu_{sr}}Z + g_{1,0}^{0,1}\hat{\nu_{rs}}Z + \cdots + g_{2,1}^{0}Z^2\bar{Z} + \cdots + g_{2,1}^{1,0}\hat{\nu_{sr}}Z^2\bar{Z} + \cdots \tag{19}$$

where we search for the coefficients $g_{1,0}^{1,0} \neq 0$, $g_{1,0}^{0,1} \neq 0$ and $g_{2,1}^{0} \neq 0$. To simplify the equations we reformulate in terms of polar coordinates:

$$Z = re^{i\phi}, \quad r \in \mathbb{R}^+, \quad \phi \in \mathbb{R}/2\pi\mathbb{Z}$$

Substituting into equation (18) results in the following

$$\begin{cases} e^{i\phi}\frac{dr}{dt} + ire^{i\phi}\frac{d\phi}{dt} = i\sqrt{\alpha\beta}re^{i\phi} + g_{1,0}^{1,0}\hat{\nu_{sr}}re^{i\phi} + g_{1,0}^{0,1}\hat{\nu_{rs}}re^{i\phi} + g_{2,1}^{0}r^3e^{i\phi} + h.o.t \\ e^{i\phi}\frac{dr}{dt} - ire^{i\phi}\frac{d\phi}{dt} = i\sqrt{\alpha\beta}re^{i\phi} + g_{0,1}^{1,0}\hat{\nu_{sr}}re^{i\phi} + g_{0,1}^{0,1}\hat{\nu_{rs}}re^{i\phi} + g_{1,2}^{0}r^3e^{i\phi} + h.o.t \end{cases} \tag{20}$$

Note that proving persistence of periodic solutions is beyond the scope of this work and hence we ignore higher order terms. Solving the above equations (20) with respect for $\frac{dr}{dt}$ and $\frac{d\phi}{dt}$ we get

$$\begin{cases} \frac{dr}{dt} = \frac{g_{1,0}^{1,0}+g_{0,1}^{1,0}}{2}\hat{\nu_{sr}}r + \frac{g_{1,0}^{0,1}+g_{0,1}^{0,1}}{2}\hat{\nu_{rs}}r + \frac{g_{2,1}^{0}+g_{1,2}^{0}}{2}r^3 \\ \frac{d\phi}{dt} = \sqrt{\alpha\beta} + \frac{g_{1,0}^{1,0}-g_{0,1}^{1,0}}{2i}\hat{\nu_{sr}}r + \frac{g_{1,0}^{0,1}-g_{0,1}^{0,1}}{2i}\hat{\nu_{rs}}r + \frac{g_{2,1}^{0}-g_{1,2}^{0}}{2i}r^2 \end{cases} \tag{21}$$

We introduce the following constants $c_{10}^r = \frac{g_{1,0}^{1,0}+g_{0,1}^{1,0}}{2} \Leftrightarrow Re(g_{1,0}^{0,1})$, $c_{10}^i = \frac{g_{1,0}^{1,0}-g_{0,1}^{1,0}}{2i} \Leftrightarrow Im(g_{1,0}^{1,0})$, $c_{01}^r = Re(g_{1,0}^{0,1})$, $c_{01}^i = Im(g_{1,0}^{0,1})$, $c_{12}^r = Re(g_{1,2}^{0})$ and $c_{12}^i = Im(g_{1,2}^{0})$. Since the above equations (21) are now decoupled we can first solve for r and by quadrature solve for ϕ. Furthermore in equation (21), $\frac{dr}{dt}$ defines the normal form for either the supercritical (subcritical) pitchfork bifurcation dependent on whether the sign of c_{12}^r is positive (negative) respectively and the equilibrium points are given by

$$r^* = \pm\sqrt{\frac{\hat{\nu_{sr}}c_{10}^r + \hat{\nu_{rs}}c_{01}^r}{c_{12}^r}}, \quad r^* = 0 \tag{22}$$

In particular we search for non-trivial, stable states and these are satisfied for small $(\hat{\nu_{sr}}, \hat{\nu_{rs}})$ parameters, providing $\frac{\hat{\nu_{sr}}c_{10}^r+\hat{\nu_{rs}}c_{01}^r}{c_{12}^r} > 0$ which implies that the vector field admits in a small neighbourhood about $0 \in \mathbb{R}^2$ a unique periodic orbit with radius r^*. Substituting r^* into $\frac{d\phi}{dt}$ we obtain a stable solution ϕ^* which describes the phase of the orbit and consequently the solution is locally a periodic limit cycle defined by $Z = r^*e^{i\phi^*t}$ with period $T = \frac{2\pi}{\sqrt{\alpha\beta}}$.

4.3 Computation of the normal form

The derivation of the Homological equation is given for completeness in Appendix A.1. From the operator, we can determine the coefficients of the Taylor expansion of the reduction function $h \in C^k(E_0 \times \mathbb{R}^2; E_h)$ and the coefficients of the polynomial $G \in C^k(E_0 \times \mathbb{R}^2; E_h)$. We define the operator as follows:

$$Jh(z,\hat{\nu}) - D_z[h(z,\hat{\nu})](Jz) = G(z,\hat{\nu}) - N(z + h(z,\hat{\nu}),\hat{\nu}) + D_z[h(z,\hat{\nu})](G(z,\hat{\nu})), \tag{23}$$

where the Ansatz is defined by

$$\begin{cases} h(z,\hat{\nu}) = \sum_{\substack{\psi\in\Gamma^n \\ |\psi|>2 \\ \chi\in\Lambda^m}} h_\psi^\chi[z^\psi,\hat{\nu}^\chi] = h^\chi_{|\psi|=2} z^\psi \hat{\nu}^\chi + h^\chi_{|\psi|=3} z^\psi \hat{\nu}^\chi + \cdots, \text{with} \quad h = \mathcal{O}(|z||(z,\hat{\nu})|) \\ G(z,\hat{\nu}) = \sum_{\substack{\psi\in\Gamma^n \\ |\psi|=2n+1 \\ n\in\mathbb{N} \\ \chi\in\Lambda^m \\ (|\psi|,|\chi|)\neq(1,0)}} G_\psi^\chi[z^\psi,\hat{\nu}^\chi] = g^{|\chi|=1}_{|\psi|=1} z^\psi \hat{\nu}^\chi + g^\chi_{|\psi|=3} z^\psi \hat{\nu}^\chi + \cdots, \text{with} \quad G = \mathcal{O}(|z|(|z|^2,\hat{\nu})|) \\ N(\hat{x},\hat{\nu}) = \sum_{\substack{\psi\in\Gamma^n \\ |\psi|>2 \\ \chi\in\Lambda^m}} N_\psi^\chi[\hat{x}^\psi,\hat{\nu}^\chi] = N^\chi_{|\psi|=2} \hat{x}^\psi \nu^\chi + N^\chi_{|\psi|=3} \hat{x}^\psi \hat{\nu}^\chi + \cdots, \text{with} \quad N = \mathcal{O}(|\hat{x}||(\hat{x},\hat{\nu})|) \end{cases} \tag{24}$$

We commence by first identifying terms in equation (24) of the same order in both the coordinates and the control parameters, i.e. ($\hat{z}$,$\hat{\nu}$), and replace these in the homological equation (23). For terms that are linear in z and linear in the control parameters, that is, $\mathcal{O}(z\hat{\nu})$ we obtain the following first order homological operator

$$Jh_1^1(z,\hat{\nu}) - D_z[h_1^1(z,\hat{\nu})](Jz) = G_1^1(z,\hat{\nu}) - N_1^1(z\hat{\nu}). \tag{25}$$

Expanding and evaluating the individual terms in equation (25) and then grouping those of the same order (for details of the calculation see Appenidx §A.2) gives rise to the following four equations

$$\begin{cases} (J - i\sqrt{\alpha\beta}I)h_{1,0}^{1,0} = g_{1,0}^{1,0} e_0 - N_1^{1,0}(e_0) \\ (J - i\sqrt{\alpha\beta}I)h_{1,0}^{0,1} = g_{1,0}^{0,1} e_0 - N_1^{0,1}(e_0) \\ g_{0,1}^{1,0} = \bar{g}_{1,0}^{1,0} \\ g_{1,0}^{0,1} = \bar{g}_{0,1}^{0,1} \end{cases}. \tag{26}$$

From equation (26) we need to obtain $g_{1,0}^{1,0}$ and $g_{1,0}^{0,1}$, which are the first order coefficients of the normal form. However, the operator $(J - i\sqrt{\alpha\beta})$ is not invertible. Hence, for a solution $h_{1,0}^{1,0}$ or $h_{1,0}^{0,1}$ to exist, the right-hand side must belong to $Range(J - i\sqrt{\alpha\beta}I)$. However, $Range(J - i\sqrt{\alpha\beta}I) = Ker(J^* + i\sqrt{\alpha\beta}I)^\perp$, where J^* is the adjoint operator of J. Hence, equation (26) has a solution if the

inner product of the right hand side with $\bar{f}_0$ is zero, where $\bar{f}_0$ is the adjoint dual base of e_0 and with the following form

$$\bar{f}_0 = \begin{pmatrix} \frac{-\alpha\beta\nu^*_{rs}\frac{\partial\varsigma[V^\star_s]}{\partial\widehat{V_s}}((\alpha+\beta)^2+\alpha\beta)}{-\alpha\beta(\alpha+\beta)+i\sqrt{\alpha\beta}(\alpha+\beta)^2} \\ \frac{\nu^*_{rs}\frac{\partial\varsigma[V^\star_s]}{\partial\widehat{V_s}}(\alpha\beta-i\sqrt{\alpha\beta}(\alpha+\beta))}{-((\alpha+\beta)^2+i\sqrt{\alpha\beta}(\alpha+\beta))} \\ -i\sqrt{\alpha\beta} \\ 1 \end{pmatrix}. \tag{27}$$

Thus to obtain the coefficients $g^{1,0}_{1,0}$ and $g^{0,1}_{1,0}$ we project every term of equation (26) onto the following space $Ker(J^* + i\sqrt{\alpha\beta}I)^\perp$, which corresponds to applying the following procedure

$$\begin{cases} < (J - i\sqrt{\alpha\beta}I)h^{1,0}_{1,0}, \bar{f}_0 >= g^{1,0}_{1,0} < e_0, \bar{f}_0 > - < N^{1,0}_1(e_0), \bar{f}_0 > \\ < (J - i\sqrt{\alpha\beta}I)h^{0,1}_{1,0}, \bar{f}_0 >= g^{0,1}_{1,0} < e_0, \bar{f}_0 > - < N^{0,1}_1(e_0), \bar{f}_0 > \end{cases} \tag{28}$$

where $< \cdot\,, \cdot >$ denotes the inner product of two vectors. Using the facts that for any vectors $a, b \in \mathbb{C}$ then $< Ja, b >=< a, J^*b >$ and $< \lambda a, b >=< a, \bar{\lambda}b >$ (where J is the linear operator, J^* the adjoint operator and λ an eigenvalue), then the left hand side of equation (28) equates to $< h^{1,0}_{1,0}, (J^* + i\sqrt{\alpha\beta}I)\bar{f}_0 >= 0$ and $< h^{0,1}_{1,0}, (J^* + i\sqrt{\alpha\beta}I)\bar{f}_0 >= 0$. Hence we have that

$$\begin{aligned} g^{1,0}_{1,0} &= \frac{< N^{1,0}_1(e_0), \bar{f}_0 >}{< e_0, \bar{f}_0 >} \\ &\Leftrightarrow -\frac{(\alpha\beta)^2\nu^*_{rs}\frac{\partial\varsigma[V^\star_s]}{\partial\widehat{V_s}}\frac{\partial\varsigma[V^\star_r]}{\partial\widehat{V_r}}}{4\alpha\beta(\alpha+\beta)+i\sqrt{\alpha\beta}(\alpha+\beta)^2}\hat{\nu_{sr}}, \end{aligned} \tag{29}$$

and for the other coefficient we also have

$$\begin{aligned} g^{0,1}_{1,0} &= \frac{< N^{0,1}_1(e_0), \bar{f}_0 >}{< e_0, \bar{f}_0 >} \\ &\Leftrightarrow -\frac{(\alpha\beta)^2\nu^*_{sr}\frac{\partial\varsigma[V^\star_s]}{\partial\widehat{V_s}}\frac{\partial\varsigma[V^\star_r]}{\partial\widehat{V_r}}}{4\alpha\beta(\alpha+\beta)+i\sqrt{\alpha\beta}(\alpha+\beta)^2}\hat{\nu_{rs}}. \end{aligned} \tag{30}$$

For the above coefficients $g^{1,0}_{1,0}$ and $g^{0,1}_{1,0}$ we are only interested in the real parts, which corresponds to a negative value in both cases. To evaluate higher order terms of the normal form, in this case the cubic terms, it turns out that we first need to resolve terms that are quadratic in the coordinates of the centre space and that have no dependence on the parameters ν, (i.e $\mathcal{O}(Z^2)$). This becomes clearer as the calculations progresses.

Thus by reducing the homological operator to quadratic terms we obtain the following

$$Jh^0_2(z) - D_z[h^0_2(z)](Jz) = -N^0_2(z, z). \tag{31}$$

From equation (31) we can determine the following coefficients (for details of this calculation see section§A.3):

$$\begin{cases} h^0_{2,0} = -(J - 2i\sqrt{\alpha\beta})^{-1} N_2(e_0, e_0) \\ h^0_{1,1} = -J^{-1} N_2(e_0, \bar{e_0}) \\ h^0_{0,2} = h^{\bar{0}}_{2,0} \end{cases} \tag{32}$$

thus we have,

$$h^0_{2,0} = \frac{-(\alpha\beta)^2 \nu_{sr}}{2! det(J - 2i\sqrt{\alpha\beta})} H, \tag{33}$$

where

$$H = \begin{pmatrix} (-3\alpha\beta + 2i\sqrt{\alpha\beta}(\alpha+\beta))[-(\alpha+\beta)^2 \frac{\partial^2 \varsigma[V_r^\star]}{\partial \widehat{V_r}^2}] + (\alpha\beta)^2 (\nu^*_{sr})^2 \nu^*_{rs} \frac{\partial^2 \varsigma[V_s^\star]}{\partial \widehat{V_s}^2} (\frac{\partial \varsigma[V_r^\star]}{\partial \widehat{V_r}})^3 \\ (\alpha\beta)(\alpha+\beta)^2 \frac{\partial^2 \varsigma[V_r^\star]}{\partial \widehat{V_r}^2} [4(\alpha+\beta) + 6i\sqrt{\alpha\beta}] + 2i\sqrt{\alpha\beta}(\alpha\beta)^2 (\nu^*_{sr})^2 \nu^*_{rs} \frac{\partial^2 \varsigma[V_s^\star]}{\partial \widehat{V_s}^2} (\frac{\partial \varsigma[V_r^\star]}{\partial \widehat{V_r}})^3 \\ -\alpha\beta(\alpha+\beta)^2 \nu^*_{rs} \frac{\partial \varsigma[V_s^\star]}{\partial \widehat{V_s}} \frac{\partial^2 \varsigma[V_r^\star]}{\partial \widehat{V_r}^2} + \alpha\beta \nu^*_{rs} \nu^*_{sr} \frac{\partial^2 \varsigma[V_s^\star]}{\partial \widehat{V_s}^2} (\frac{\partial \varsigma[V_r^\star]}{\partial \widehat{V_r}})^2)[-3\alpha\beta + 2i\sqrt{\alpha\beta}(\alpha+\beta)] \\ -2i\sqrt{\alpha\beta}(\alpha\beta)(\alpha+\beta)^2 \nu^*_{rs} \frac{\partial \varsigma[V_s^\star]}{\partial \widehat{V_s}} \frac{\partial^2 \varsigma[V_r^\star]}{\partial \widehat{V_r}^2} - 2(\alpha\beta)^2 \nu^*_{rs} \nu^*_{sr} \frac{\partial^2 \varsigma[V_s^\star]}{\partial \widehat{V_s}^2} (\frac{\partial \varsigma[V_r^\star]}{\partial \widehat{V_r}})^2 [2(\alpha+\beta) + 3i\sqrt{\alpha\beta}] \end{pmatrix},$$

and $det(J - 2i\sqrt{\alpha\beta}) = 3\alpha\beta(((\alpha^2+\beta^2)+\alpha\beta) + 4i\sqrt{\alpha\beta}(\alpha+\beta))$. For the other coefficient we have the following

$$h^0_{1,1} = \frac{(\alpha\beta)^2 \nu^*_{sr}}{2![(\alpha+\beta)^2 + \alpha\beta]} \begin{pmatrix} (\alpha+\beta)^2 \frac{\partial^2 \varsigma[V_r^\star]}{\partial \widehat{V_r}^2} + (\alpha\beta) \frac{\partial^2 \varsigma[V_s^\star]}{\partial \widehat{V_s}^2} (\frac{\partial \varsigma[V_r^\star]}{\partial \widehat{V_r}})^3 \nu^*_{rs} (\nu^*_{sr})^2 \\ 0 \\ \nu^*_{rs}[(\alpha+\beta)^2 \frac{\partial \varsigma[V_s^\star]}{\partial \widehat{V_s}} \frac{\partial^2 \varsigma[V_r^\star]}{\partial \widehat{V_r}^2} + (\alpha\beta) \nu^*_{sr} \frac{\partial^2 \varsigma[V_s^\star]}{\partial \widehat{V_s}^2} (\frac{\partial \varsigma[V_r^\star]}{\partial \widehat{V_r}})^2] \\ 0 \end{pmatrix}. \tag{34}$$

Having evaluated the quadratic coefficients we may now resolve terms that are cubic in the coordinates of the centre space and that have no dependence on the control parameters, which are precisely the coefficients for the unfolding of a Hopf bifurcation. Reducing the homological operator to cubic terms we obtain the following:

$$J h^0_3(z) - D_z[h^0_3(z)](Jz) = G^0_3 - 2N^0_2(z, h^0_2(z)) - N_3(z, z, z). \tag{35}$$

By expanding the individual terms in the homological operator and grouping the terms of the following order $Z^2\bar{Z}$, $Z\bar{Z}^2$,Z^3 and $\bar{Z}^3$ we obtain four equations (details of the calculations can be found in section §A.4). However, for the Hopf bifurcation we can restrict to those equations that depend on $Z\bar{Z}^2$, $Z^2\bar{Z}$, giving the following:

$$\begin{cases} (L - i\sqrt{\alpha\beta} I) h^0_{2,1} = g^{0,0}_{2,1} e_0 - 2N^0_2(\bar{e_0}, h^{0,0}_{2,0}) - 2N^0_2(e_0, h^{0,0}_{1,1}) - 3N^0_3(e_0, e_0, \bar{e_0}) \\ g^{0,0}_{1,2} = \bar{g}^{0,0}_{2,1} \end{cases} \tag{36}$$

From equation (36) we need to evaluate $g_{1,2}^{0,0}$ and $g_{2,1}^{0,0}$. Again noting that the operator $(J - i\sqrt{\alpha\beta}I)$ is not invertible we employ the same procedure as performed for the first order terms, that is, to apply the inner product to all the terms of equation (36) with the adjoint dual base of e_0 which we denoted then by $\bar{f}_0$. Hence we obtain the following:

$$\begin{aligned} < (L - i\sqrt{\alpha\beta}I)h_{2,1}^0, \bar{f}_0 > &= g_{2,1}^{0,0} < e_0, \bar{f}_0 > -2 < N_2^0(\bar{e_0}, h_{2,0}^{0,0}), \bar{f}_0 > -2 < N_2^0(e_0, h_{1,1}^{0,0}), \bar{f}_0 > \\ &- 3 < N_3^0(e_0, e_0, \bar{e_0}), \bar{f}_0 > . \end{aligned} \quad (37)$$

The left hand side of equation (37) equates to $< (L - i\sqrt{\alpha\beta}I)h_{2,1}^0, \bar{f}_0 > \Leftrightarrow < h_{2,1}^0, (J^* + i\sqrt{\alpha\beta}I)\bar{f}_0 > = 0$, thus resulting in the following cubic coefficient for the Hopf bifurcation

$$g_{1,2}^{0,0} = \frac{2 < N_2^0(\bar{e_0}, h_{2,0}^{0,0}), \bar{f}_0 > +2 < N_2^0(e_0, h_{1,1}^{0,0}), \bar{f}_0 > +3 < N_3^0(e_0, e_0, \bar{e_0}), \bar{f}_0 >}{< e_0, \bar{f}_0 >} \quad (38)$$

Once again, we are only interested in the real part, resulting in the following:

$$c_{12}^r = Re(g_{1,2}^{0,0}) = -\frac{(\alpha\beta)^3 \nu_{sr}^* \nu_{rs}^* (c1 + c2 + c3)}{2!3[(\alpha^2 + \alpha\beta + \beta^2)^2 + 16\alpha\beta(\alpha+\beta)^2][(\alpha+\beta)^2 + \alpha\beta][(\alpha+\beta)^2 + \alpha\beta](\alpha+\beta)}, \quad (39)$$

where $c1$ corresponds to

$$\begin{aligned} c1 &= 2((\alpha+\beta)^2 + \alpha\beta) \left(2(\alpha\beta)^2(\alpha+\beta)^3 \nu_{rs}^* \nu_{sr}^* (\frac{\partial^2 \varsigma[V_r^\star]}{\partial \widehat{V_r}^2})^2 (\frac{\partial \varsigma[V_s^\star]}{\partial \widehat{V_s}})^2 \right. \\ &+ 6(\nu_{sr}^* - 1)(\alpha\beta)^2(\alpha+\beta)^2 \frac{\partial \varsigma[V_r^\star]}{\partial \widehat{V_r}} \frac{\partial^2 \varsigma[V_r^\star]}{\partial \widehat{V_r}^2} \frac{\partial^2 \varsigma[V_s^\star]}{\partial \widehat{V_s}^2} \\ &+ (\alpha\beta)^2 (\nu_{sr}^*)^3 \nu_{rs}^* (-6(\alpha\beta)^2 + (\alpha+\beta)^2) (\frac{\partial^2 \varsigma[V_s^\star]}{\partial \widehat{V_s}^2})^2 (\frac{\partial \varsigma[V_r^\star]}{\partial \widehat{V_r}})^4 \\ &+ \left. \nu_{sr}^* (\alpha+\beta)^4 ((\alpha+\beta)^2 + 15\alpha\beta) [\frac{\partial \varsigma[V_r^\star]}{\partial \widehat{V_r}} - \frac{\partial \varsigma[V_s^\star]}{\partial \widehat{V_s}}] \right), \end{aligned}$$

and the constant $c2$:

$$\begin{aligned} c2 &= 12\alpha\beta\nu_{sr}^* [(\alpha^2 + \alpha\beta + \beta^2)^2 + 16\alpha\beta(\alpha+\beta)^2] \left(\nu_{rs}^* \frac{\partial^2 \varsigma[V_r^\star]}{\partial \widehat{V_r}^2} \frac{\partial \varsigma[V_s^\star]}{\partial \widehat{V_s}} \left[(\alpha+\beta)^2 \frac{\partial \varsigma[V_s^\star]}{\partial \widehat{V_s}} \frac{\partial^2 \varsigma[V_r^\star]}{\partial \widehat{V_r}^2} \right. \right. \\ &+ \left. \alpha\beta\nu_{sr}^* \frac{\partial^2 \varsigma[V_s^\star]}{\partial \widehat{V_s}^2} (\frac{\partial \varsigma[V_r^\star]}{\partial \widehat{V_r}})^2 \right] + \frac{\partial^2 \varsigma[V_s^\star]}{\partial \widehat{V_s}^2} \frac{\partial \varsigma[V_r^\star]}{\partial \widehat{V_r}} \left[(\alpha+\beta)^2 \frac{\partial^2 \varsigma[V_r^\star]}{\partial \widehat{V_r}^2} \right. \\ &+ \left. \left. \alpha\beta(\nu_{sr}^*)^2 \nu_{rs}^* \frac{\partial^2 \varsigma[V_s^\star]}{\partial \widehat{V_s}^2} (\frac{\partial \varsigma[V_r^\star]}{\partial \widehat{V_r}})^3 \right] \right). \end{aligned}$$

Finally the constant $c3$ has the following form

$$\begin{aligned} c3 &= 12[(\alpha^2 + \alpha\beta + \beta^2)^2 + 16\alpha\beta(\alpha+\beta)^2]((\alpha+\beta)^2 + \alpha\beta) \left((\alpha+\beta)^2 \frac{\partial^3 \varsigma[V_r^\star]}{\partial \widehat{V_r}^3} \frac{\partial \varsigma[V_s^\star]}{\partial \widehat{V_s}} \right. \\ &+ \left. \alpha\beta(\nu_{sr}^*)^2 \frac{\partial^3 \varsigma[V_s^\star]}{\partial \widehat{V_s}^3} (\frac{\partial \varsigma[V_r^\star]}{\partial \widehat{V_r}})^3 \right). \end{aligned}$$

Since α and β are both positive, ν_{sr}^* is negative and so is the sum of $c1, c2$ and $c3$, we can conclude that c_{12}^r is negative. This implies that the system exhibits a supercritical Hopf bifurcation, confirming the numerical results of section 3.1. Furthermore, the reduction function $h(z)$ is composed by the quadratic coefficients $h_{2,0}^0$, $h_{1,1}^0$ and $h_{0,2}^0$.

5 Global analysis of limit cycles in the piecewise linear model

Having used the normal forms to determine analytically local stability results, we now progress to consider global stability of limit cycles. A piecewise linear version of system (1) is formulated and global stability for a restricted region of the parameter space is proven. The approach chosen to study global properties of the limit cycle is developed from the theory, *Constructive Global Analysis of Hybrid Systems* [16]. The formalism is based on *Piecewise Linear Systems* (PLS) which are characterized by three components; a set of *affine linear systems*; a *switching rule* to switch among them, which depends on present values of x and possibly on past values of the state and *switching surfaces* consisting of hyper-planes of dimension $n-1$ defined respectively as:

$$\begin{cases} \dot{x} = A_\alpha x + B_\alpha, \quad x \in \mathbb{R}^n \\ \alpha(x) \in \{1, \cdots, M\} \\ S_J = \{x | C_J x + d_j = 0\}, \quad j = \{1, \cdots, N\} \end{cases} \tag{40}$$

This work only considers switching rules that only depend on the present values of the state x. In such case the state space is partitioned into M (possibly unbounded) sets called *cells* defined as $U_i = \{x | \alpha(x(t)) = i\}$ with $i = \{1, \cdots, M\}$ such that $U_i \cap U_j = \emptyset$, $i \neq j$. Altogether there are $M \times N$ boundaries. In each cell, U_i, the system dynamics is given by a linear system $\dot{x} = A_i x + B_i$. A solution of (40), is a function $(x(t), \alpha(x(t)))$ satisfying (40), where $x(t)$ is simply the flow of the affine system within a cell and $\alpha(x(t))$ is piecewise constant. t is the *switching time* of a solution of (40) if $\alpha(t)$ is discontinuous a t. This paper assumes that existence of solution is always guaranteed for any initial condition (see [28] for conditions on existence of solutions for PLS). Unlike linear systems that only have a single equilibrium point, PLS may exhibit multiple equilibrium points and/or limit cycles. Our focus is to determine the conditions that give rise to limit cycles on the piecewise linear version of the RKII set and to show global stability of these oscillations. In particular the existence of limit cycles of a PLS is given by the following proposition (see details of the proof in [16]):

Proposition 1 (Existence of Limit Cycles for PLS)**.** *Consider the PLS. Suppose that there exists a limit cycle γ with k switches per cycle and with period $t^* = t_1^* + t_2^* + \cdots + t_k^* > 0$. Then the following*

conditions hold:

$$g_k(t_1^*,\dots,t_k^*) = C_k(I - E_k\dots E_1)^{-1}\left[\sum_{i=1}^{k-1} E_k\dots E_{i+1}(E_i - I)z_i + (E_k - I)z_k\right] - d_k = 0,$$

where $E_i = e^{A_i t_i^*}$ *and* $z_i = A_i^{-1}B_i$. *The periodic orbit is governed by system* 1 *on* $[0, t_1^*)$, *and the by the system* i *on* $[t_1^* + \dots + t_{i-1}^*, t_1^* + \dots + t_i^*)$, $i = 2,\dots,k$. *Furthermore, the periodic solution* γ *can be obtained with the initial condition* $x_0^* \in S_k$

$$x_0^* = (I - E_k\dots E_1)^{-1}\left[\sum_{i=1}^{k-1} E_k\dots E_{i+1}(E_i - I)z_i + (E_k - I)z_k\right].$$

Global stability can be determined by showing that system trajectories are globally contracting to a fixed point on the switching surfaces. This is made possible by the study of impact maps. To make things clear consider system (40) where we only analyse locally the flow from switching surface S_1 to S_2. Let both S_1 and S_2 be defined on the boundaries of subset of cell $U \in \mathbb{R}^n$ and the linear time invariant system $\dot{x} = A_0x + B_0$, $x \in U$ is allowed to have stable, unstable or pure imaginary eigenvalues. Define the *departure set* $S_1^d \subset S_1$ where any trajectory starting at S_1^d satisfies $x(t) \in S_2$, for some finite *switching time* $t \geq 0$, and $x(\tau) \in U^*$ on $[0, t]$, where U^* is the *closure* of U (i.e $U^* = U \cup \{x|\text{x is a limit point U}\}$). Let the *arrival set* $S_2^a \subset S_2$ be the set of those points $x_2 = x(t)$, that is, the image of S_1^d. Any point belonging to the switching surface $x_1 \in S_1^d$ and $x_2 \in S_2^a$ can be parameterised in their respective hyperplanes. For that, let $x_1 = x_1^* + \Delta_1$ and $x_2 = x_2^* + \Delta_2$, where $x_1^* \in S_1$, $x_2^* \in S_2$ and Δ_1, Δ_2 are any vectors such that $\Delta_1 \in S_1^d - x_1^*$ and $\Delta_2 \in S_2^a - x_2^*$. In this case $C_1\Delta_1 = C_2\Delta_2 = 0$. The impact map then reduces to the study of a map from Δ_1 to Δ_2. However, since the map is multi-valued (i.e. the same initial condition Δ_1 can have multiple switching times) the following definition is introduced (see [16] for details):

Definition 1 (Expected switching times)**.** *Let* $x(0) = x_1^* + \Delta_1$. *Define* t_{Δ_1} *as the set of all times* $t_i \geq 0$ *such that the trajectory* $x(t)$ *with initial condition* $x(0)$ *satisfies* $C_2x(t_i) = d_2$ *and* $x(t) \in U^*$ *on* $[0, t_i]$. *Define also the set of expected switching times of the impact map from* $\Delta_1 \in S_1^d - x_1^*$ *to* $\Delta_2 \in S_2^a - x_2^*$ *as*

$$\mathcal{T} = \{t | t \in t_{\Delta_1}, \Delta_1 \in S_1^d - x_1^*\}.$$

In general a map between switching surfaces is nonlinear, however a map induced by a linear time invariant flow, can be represented as *linear transformation* analytically parameterized by a scalar function

of the state (in this case the switching times t_{Δ_i}) and this is given by the following Theorem (proven in [16]):

Theorem 1 (Impact Map). *Assume $C_2 x_1^*(t) \neq d_2$ for all $t \in \mathcal{T}$. Define the transition function as*

$$\begin{cases} H(t) = e^{At} + (x_1^*(t) - x_2^*)w(t), \quad H(t) : \mathbb{R} \to \mathbb{R}^{n-1}, \\ w(t) = \frac{C_2 e^{At}}{d_2 - C_2 x_1^*(t)}. \end{cases}$$

Then, for any $\Delta_1 \in S_1^d - x_1^*$ there exists a $t \in \mathcal{T}$ such that the impact map is given by

$$\Delta_2 = H(t)\Delta_1,$$

such $t \in t_{\Delta_1}$ is the switching time associated with Δ_2.

From the above theorem it is clear that Δ_1 is a nonlinear function of Δ_2. However, fixing the switching time t determines the set of points $x_1^* + \Delta_1 \in S_0$ such that every point in that set has a switching time t. In this view the map is linear. Furthermore, the set of points S_1^d that have a switching time t is a convex subset of a linear manifold of dimension $n-2$ which is denoted as S_t and defined as $S_t = \{t | t \in t_{\Delta_1}, x_1^* + \Delta_1 \in S_1^d\}$. Note that since the impact map is multi-valued, a point S_1^d may belong to more than one set S_t. Also as $t \in \mathcal{T}$ changes, S_t covers every single point of S_1^d, i.e $S_0^d = \{x | x \in S_t, t \in \mathcal{T}\}$. Finally note that the above theorem states that a trajectory cannot intersect the switching surface S_2 for all $t \in \mathcal{T}$. It is then possible to prove global stability by constructing surface quadratic Lyapunov functions V_1 and V_2 on the switching surfaces S_1^d and S_2^a and then showing that the impact maps from S_1^d to S_2^a are quadratically stable. This is made possible by demonstrating the following global stability theorem for impact maps is satisfied (see proof in [16]):

Theorem 2 (Stability of impact map). *Define*

$$R(t) = P_1 - H(t)^T P_2 H(t) - 2(g_1 - H(t)^T g_2)w_t + w_t^T(\alpha_1 - \alpha_2)w_t \tag{41}$$

The impact map from $\Delta_1 \in S_1^d - x_1^*$ to $\Delta_2 \in S_2^a - x_2^*$ is quadratically stable if and only if there exist P_1, $P_2 > 0$ and g_1, g_2, α_1,α_2 such that

$$R(t) > 0 \quad S_t - x_1^*, \tag{42}$$

for all expected switching times $t \in \mathcal{T}$.

Thus, if the above piecewise linear system (40) exhibits a limit cycle (i.e. having trajectories from S_1 to S_2 and in turn from S_2 to S_1) then it is first necessary to determine SuLF on S_1 and S_2. Once the

quadratic functions are determined it is easy to show that the limit cycle is stable or not by applying Theorem (2) which proves that the impact maps S_1 to S_2 and from S_2 to S_1 are contracting. In other words, the trajectories contract to a global stable fixed point in the hyper-planes.

5.1 Analysis of piecewise linear RKII set

In the following sections we will present results for a piecewise linear version of the RKII model (1). The model (1) can be reformulated in the form of a LTI system where usually the model is essentially separated into linear and nonlinear terms and can be re-written in the following form

$$\begin{cases} \dot{x} = Ax + Bu \\ y = Cx + Du \end{cases}$$

where $x = (V_s, w, V_r, v)$. The matrix A contains only linear terms, while B contains the coefficients of the nonlinear and the forcing terms, in the case of model (1), u corresponds to the sigmoidal functions. $y = Cx + Du$ denotes the output equation where for this case we have $D = 0$ (the feed matrix). The matrix A is defined as follows:

$$A = \begin{pmatrix} \tilde{A} & 0 \\ 0 & \tilde{A} \end{pmatrix} \quad , \quad \tilde{A} = \begin{pmatrix} 0 & 1 \\ -\alpha\beta & -(\alpha+\beta) \end{pmatrix}$$

Note that A is invertible and all the eigenvalues lie in the left half plane. The definition of matrix B and u, and consequently the switching surfaces will depend on the specific form of the piecewise approximation of the nonlinear functions. Here we will first investigate the approximation of the saturating function $\varsigma[V_a(t)]$ by a Heaviside function. The original saturating function is unipolar (i.e. it assumes only positive values), but for the purpose of this discussion and generality we will neglect this limitation and will assume that it may also attain negative values. Thus we define the Heaviside function as follows:

$$u = \Theta(y - \theta) = \begin{cases} a & y \leq \theta, \\ b & otherwise \end{cases}$$

where we assume that $(a, b, \theta) \in \mathbb{R}$. Since we have saturating functions dependent on the dynamic variables V_s and V_r we can define an approximation for each function independently, thus allowing for more general results. Further, we define two switching surfaces (one for each function), by allowing the LTI flow from lower asymptote (a) to the upper asymptote (b) of the Heaviside function. Hence, the

complete formulation is as follows:

$$\begin{cases} \dot{x} = Ax + \tilde{B}_0\tilde{u_0} + \tilde{B}_1\tilde{u_1} + \tilde{B}_2\tilde{u_2} \Leftrightarrow Ax + Bu \\ y = C_0x \\ y = C_1x \end{cases}$$

where $C_0 = [0, 0, 1, 0]^T$, $C_1 = [1, 0, 0, 0]^T$ and

$$\tilde{u_i} = \Theta_i(y - \theta_i) = \begin{cases} a_i & y \leq \theta_i, \\ b_i & otherwise \end{cases}$$

with $i = \{0, 1\}$ and the vector $u = [\tilde{u_0}, \tilde{u_1}, \tilde{u_2}]^T$. Note $\tilde{u_2}$ is due to the ϕ_n term in system (1) and here we consider a constant term, $\phi_n = 1$. The matrix B is then defined as

$$B = \begin{pmatrix} 0 & 0 & 0 \\ \alpha\beta\nu_{sr} & 0 & \alpha\beta\nu_{sn} \\ 0 & 0 & 0 \\ 0 & \alpha\beta\nu_{rs} & 0 \end{pmatrix}.$$

Since A is invertible, the equilibrium of $\dot{x} = Ax + Bu$ can be readily evaluated as $x^* = -A^{-1}Bu$ and has the following form

$$\mathbf{x}^* = \begin{pmatrix} \nu_{sr}\tilde{u_0} + \nu_{sn}\tilde{u_2} \\ 0 \\ \nu_{rs}\tilde{u_1} \\ 0 \end{pmatrix}$$

where

$$A^{-1} = \begin{pmatrix} \widehat{A} & 0 \\ 0 & \widehat{A} \end{pmatrix} \quad , \quad \widehat{A} = \begin{pmatrix} \frac{-(\alpha+\beta)}{\alpha\beta} & \frac{-1}{\alpha\beta} \\ 1 & 0 \end{pmatrix}$$

A schematic of the reformulated model is depicted in Fig. 5.

Furthermore the two switching surfaces (hyperplanes in $\mathbb{R}^3$) are defined as follows

$$S_0 = \{x \in \mathbb{R}^4 : C_0x = \theta_0\} \quad \text{and} \quad S_1 = \{x \in \mathbb{R}^4 : C_1x = \theta_1\}$$

Since we have two switching surfaces it means that the projection onto the (V_s, V_r) state space is divided into four regions, where the dynamics of each region is governed by a separate system of the form $\dot{x}_i = Ax + Bu_i$ with $i \in \{1, 2, 3, 4\}$. We denote each of these by System$_i$. Fig. 6 depicts the above and from this we can derive the conditions for the existence of a globally stable limit cycle.

The existence of a limit cycle depends on several different factors, for example whether or not the matrix A for each system is stable or not, and in which region the equilibrium of each system lies. Depending on the location of the equilibrium points, the model may give rise to rich and complicated dynamics and even chaotic behavior. Finally the initial conditions also play an important role. If the matrix A of each system is stable then a limit cycle can occur if each system has an equilibrium point in a different region. That is, for example, System$_1$ (in the third quadrant) must not have its equilibrium in the third quadrant. If System$_1$ contains its equilibrium elsewhere (except region 3), then the LTI flow will intersect a hyperplane S_0 or S_1 at some finite time moment t^* when the governing equations of some other system will take over (in this case either system 2 or 4) and the same scenario could repeat until a closed trajectory is formed. However, it is important to note that this scenario does not guarantee a limit cycle as the system can be chaotic. On the other hand, if matrix A was unstable it could happen that all systems have equilibrium points in their own region, however the overall model posseses a limit cycle, since they would be unstable equilibrium and so depend on the initial conditions.

In general, solving the existence conditions for limit cycles can be hard (as it involves exponential matrices and transcendental equations), however using proposition (1) allows for example to simulate the system and obtain switching times and intersection points when the trajectory traverses a switching surface. This information then permits verification of the stability of a limit cycle. For our model in particular, we have that matrix A is stable (having all its eigenvalues on the left half plane), thus all of the four systems are stable. However, the equilibrium state of each system lies in a different region, due to the different vectors u_i, with $i \in \{1, 2, 3, 4\}$. For ease of derivation of the limit cycle conditions we denote Bu_i as simply B_i.

Making use of Fig. 6 we can state the following necessary conditions for the appearance of the limit cycles:

Proposition 2. *The switching surfaces S_0 and S_1 (governed respectively by the equations of the hyperplanes C_0x and C_1x) divide the state space (V_s, V_r) into four regions, each of which having an independent LTI flow $x_i = Ax + B_i$ with $i \in \{1, 2, 3, 4\}$. Since A is a stable matrix, then the existence of a globally stable limit cycle is only true if the following necessary conditions are satisfied:*

1. *System 1:* $-C_0A^{-1}B_1 > \theta_0$ *or* $-C_1A^{-1}B_1 > \theta_1 = \{\ \nu_{rs}a_1 > \theta_0$ *or* $u_{sr}a_0 + \phi_n\nu_{sn} > \theta_1\ \}$
2. *System 2:* $-C_0A^{-1}B_2 > \theta_0$ *or* $-C_1A^{-1}B_2 < \theta_1 = \{\ \nu_{rs}b_1 > \theta_0$ *or* $\nu_{sr}a_0 + \phi_n\nu_{sn} < \theta_1\ \}$
3. *System 3:* $-C_0A^{-1}B_3 < \theta_0$ *or* $-C_1A^{-1}B_3 < \theta_1 = \{\ \nu_{rs}b_1 < \theta_0$ *or* $\nu_{sr}b_0 + \phi_n\nu_{sn} < \theta_1\ \}$

4. *System 4:* $-C_0A^{-1}B_4 < \theta_0$ *or* $-C_1A^{-1}B_4 > \theta_1 = \{\ \nu_{rs}a_1 < \theta_0$ *or* $\nu_{sr}b_0 + \phi_n\nu_{sn} > \theta_1\ \}$

To study the local and global stability of a limit cycle we select from the numerical results of section 3.1, a region of interest in parameter space. Without lose of generality, we choose a band centered in HB1 (see Table 2) with small variations in the parameter ν_{sr} and the parameter ν_{rs} is allowed to vary freely. In this parameter window we verify that the dynamic variable V_r is always positive and gradually turns its dynamics from sub-threshold to supra-threshold as ν_{rs} is increased (where the threshold in the nonlinear function is θ). Note, there are numerous ways for determining a reasonable approximation to the nonlinear function. For example, one easy way is to generate the time series of the dynamic variables and use those as input to the nonlinear functions. Thus, the method allows us to determine what region of the nonlinear function space is being visited. The approximation chosen for V_r in this parameter regime is a Heaviside function with parameters $(a_0, b_0, \theta_0) = (0, 250, 0.015)$, for this case θ_0 coincides with the threshold of the sigmoidal function. Conversely V_s has only sub-threshold dynamics occupying mostly the lower asymptote of the nonlinear function. As we have seen, the sigmoidal function considered here is very steep indeed and a small variation in the input has dramatic changes in the output, so the approximation must be chosen carefully. Since V_s lies mostly on the lower asymptote we could use a function of the form $u(t) = max\{0, Cx + \theta_1\}$, where C is some vector. However, for the purpose of demonstrating global stability a simpler function will suffice. A reasonable choice is a Heaviside with the parameters $(a_1, b_1, \theta_1) = (0, 250, -0.015)$. As an example, we present a simulation using a MATLAB code we developed using the *symbolic math toolbox* (see Fig 7).

The code uses the ideas discussed where then a limit cycle is generated and the switching times and the Poincar$\acute{e}$ surface coordinates are determined. Here the code is run with the initial conditions $x_0^* = [0, 0, 0, 0]^T$ and with the control parameters fixed to (ν_{sr}, ν_{rs},ν_{sn}) =(-0.008, 0.006, 0). We observe a limit cycle in the clock-wise direction where we can easily interpret the results using the derived necessary conditions from Proposition 1. In this simulation System$_2$ in the second quadrant starts running and its trajectory tends towards its equilibrium point which lies in the first quadrant. As it evolves, a switch occurs at S_0 where then System$_1$ takes over and the same scenario for the other systems repeats as the limit cycle develops. The code is run long enough until the switching times reaches a tolerance ($|t_i^* - t| < TOL$, where TOL is some time parameter). The switching times and Poincar$\acute{e}$ surface coordinates are stored in Table 3.

5.2 Limit Cycle γ with period t^*

Here we make use of the proofs for the existence of limit cycles given by proposition (1) which provides an algorithm to derive the analytical solution of the trajectory of a limit cycle. From the numerical simulation we observe that the trajectory $\phi(t)$ of the limit cycle γ traverses each switching surface S_k with $k \in \{0, 1\}$ twice, in a sequential manner. We here denote S_k^i as the subsection of a switching surface S_k where the trajectory first intersects it and t_i^* as the time moment of the intersection, where $i = j \bmod 4$, with $j \in \mathbb{N}_0^+$. For example, S_0^0 is the subsection of the switching surface S_0 where the trajectory traverses it at time instant t_0^* (since it is a limit cycle we consider $t_0^* = t_4^*$ since $t_i^* = t_{j \bmod 4}^*$). Hence the limit cycle γ starting at the some initial condition $x_i^* \in S_k^i$ has period $t^* = t_1^* + t_2^* + t_3^* + t_4^*$ and satisfies:

i $\phi(t_1^*) = x_1^* \in S_1^1$

ii $\phi(t_1^* + t_2^*) = x_2^* \in S_0^2$

iii $\phi(t_1^* + t_2^* + t_3^*) = x_3^* \in S_1^3$

iv $\phi(t_1^* + t_2^* + t_3^* + t_4^*) = x_4^* \in S_0^0$

where each System$_i$ has a solution of the following form

$$x(t)_i = e^{At}(x_0 + A^{-1}B_i) - A^{-1}B_i.$$

From proposition (1) the piecewise trajectory $\phi(t)$ is governed by the following switching conditions

$$\begin{cases} g_0(t_1^*, t_2^*, t_3^*, t_4^*) = C_0 x_0^* - \theta_0 = 0 \\ g_1(t_1^*, t_2^*, t_3^*, t_4^*) = C_1 x_1^* - \theta_1 = 0 \\ g_2(t_1^*, t_2^*, t_3^*, t_4^*) = C_0 x_2^* - \theta_0 = 0 \\ g_3(t_1^*, t_2^*, t_3^*, t_4^*) = C_1 x_3^* - \theta_1 = 0 \end{cases}$$

where C_0 and C_1 are the output matrix (describing the hyperplanes) defined in the previous section and the periodic solution of the piecewise linear approximation is obtained with any of the initial conditions:

$$\begin{aligned}
x_0^* &= (I - e^{A(t_4^*+t_3^*+t_2^*+t_1^*)})^{-1}\Big[e^{A(t_4^*+t_3^*+t_2^*)}(e^{At_1^*}-I)A^{-1}B_1 + e^{A(t_4^*+t_3^*)}(e^{At_2^*}-I)A^{-1}B_2 \\
&\quad e^{At_4^*}(e^{At_3^*}-I)A^{-1}B_3 + (e^{At_4^*}-I)A^{-1}B_4\Big], \\
x_1^* &= (I - e^{A(t_1^*+t_4^*+t_3^*+t_2^*)})^{-1}\Big[e^{A(t_1^*+t_4^*+t_3^*)}(e^{At_2^*}-I)A^{-1}B_2 + e^{A(t_1^*+t_4^*)}(e^{At_3^*}-I)A^{-1}B_3 \\
&\quad e^{At_1^*}(e^{At_4^*}-I)A^{-1}B_4 + (e^{At_1^*}-I)A^{-1}B_1\Big], \\
x_2^* &= (I - e^{A(t_2^*+t_1^*+t_4^*+t_3^*)})^{-1}\Big[e^{A(t_2^*+t_1^*+t_4^*)}(e^{At_3^*}-I)A^{-1}B_3 + e^{A(t_2^*+t_1^*)}(e^{At_4^*}-I)A^{-1}B_4 \\
&\quad e^{At_2^*}(e^{At_1^*}-I)A^{-1}B_1 + (e^{At_2^*}-I)A^{-1}B_2\Big], \\
x_3^* &= (I - e^{A(t_3^*+t_2^*+t_1^*+t_4^*)})^{-1}\Big[e^{A(t_3^*+t_2^*+t_1^*)}(e^{At_4^*}-I)A^{-1}B_4 + e^{A(t_3^*+t_2^*)}(e^{At_1^*}-I)A^{-1}B_1 \\
&\quad e^{At_3^*}(e^{At_2^*}-I)A^{-1}B_2 + (e^{At_3^*}-I)A^{-1}B_3\Big].
\end{aligned}$$

5.3 Local stability of Limit cycle γ

The local stability of the limit cycle can be verified by considering a Poincaré map, P, from some point $x_i^* \in S_k^i$, to the point when the trajectory returns to S_k^i. i.e $P : S_k^i \to S_k^i$ and then verifying that the Jacobian of the map has all its eigenvalues inside the unit disc. The Jacobian of the map P is derived by considering small perturbations in time and space in each intermediate switching surface and then neglecting higher order terms. The results presented in [16] is a particular case of the well known results for Local stability of limit cycles for smooth systems which uses the *characteristic multipliers* to determine their stability. As such we will not detail this discussion and refer the reader to [16] for a comprehensive discussion. The Jacobian, W, of a piecewise linear system is given by the composition of all the intermediate perturbations within each switching surface and is defined as $W = W_3W_2W_1W_0$ where,

$$W_i = \left(I - \frac{v_i C_k}{C_k v_i}\right) e^{At_i^*}.$$

Here $v_i = Ax_i^* + B_i$ and $k = i \bmod 2$. Substituting the values from Table (3) we get

$$\mathbf{W} = \begin{pmatrix} 5.47\text{e-}4 & 2.71\text{e-}06 & 9.58\text{e-}03 & 4.79\text{e-}05 \\ \text{-}2.73\text{e-}2 & \text{-}1.36\text{e-}04 & \text{-}4.79\text{e-}01 & \text{-}2.39\text{e-}03 \\ 0 & 0 & 0 & 0 \\ 2.64\text{e-}05 & 1.31\text{e-}07 & 4.62\text{e-}04 & 2.31\text{e-}06 \end{pmatrix}$$

which does indeed have all its eigenvalues inside a unit disc. We therefore conclude that the limit cycle is locally stable.

5.4 Global stability of limit cycle γ

The fundamentally new concept introduced in *Constructive Global Analysis of Hybrid Systems* [16] is to infer global dynamical properties of a system through finding quadratic Lyapunov functions on the switching surfaces. Earlier studies [29, 30] had proposed continuity of the Lyapunov functions along the switching surfaces and this result lead to the idea that the intersection of two Lyapunov functions at a switching surfaces (one from each side) defined a unique quadratic Lyapunov function on the switching surface. It is then demonstrated in [16] that a quadratic Lyapunov function on the switching surface in a PLS denoted *Quadratic Surface Lyapunov Function* (SuLF) exists and that SuLF (as opposed to searching for Lyapunov functions in the state space) is sufficient to efficiently analyse global stability of limit cycles. This follows since a PLS behaves linearly inside a region (partitioned state space). In order to analyse PLS using SuLF it is first necessary to define *impact maps* from one switching surface to the next and by combining all the impact maps associated with the PLS it is possible to infer global stability. Here we can define an *impact map* associated to the LTI flow in each of the four regions. Following Theorem (1) we define:

$$H_i(t) = e^{At} + (x_i^*(t) - x_{i+1}^*)w_i(t)$$

and for each region i the following

$$w_0(t) = \frac{C_1 e^{At}}{\theta_1 - C_1 x_0^*(t)} \quad , \quad w_1(t) = \frac{C_0 e^{At}}{\theta_0 - C_0 x_1^*(t)}$$
$$w_2(t) = \frac{C_1 e^{At}}{\theta_1 - C_1 x_2^*(t)} \quad , \quad w_3(t) = \frac{C_0 e^{At}}{\theta_0 - C_0 x_3^*(t)}$$

where (i, k) have been defined above. For every impact map i define for a given initial condition in S_k^i a set of all expected switching times $t_i \in \mathcal{T}_i$. Then for any $\Delta_i \in S_k^i - x_i^*$ there exist a set of expected switching times $t_i \in \mathcal{T}_i$ such that the impact maps are given by

$$\Delta_{i+1} = H_i(t_{i+1})\Delta_i$$

where each t_i is the switching time associated to each perturbation Δ_i. Furthermore, parameterising the impact map with t_i defines the set of initial conditions $S^k_{t_i} \in S^i_k$ in a given switching surface that have the same switching time. This set of initial conditions $S^k_{t_i}$ is a convex subset of a linear manifold of dimension $n-2$ (in our case an $\mathbb{R}^2$ *surface*). To show that these four impact maps are contracting in some sense, define a SuLF on each S^i_k given by

$$V_i(x) = x^T P_i x - 2x^T g_i + \alpha_i.$$

Global asymptotically stability of the limit cycle follows if there exists $P_i > 0$ (Positive definite), g_i, α_i, such that

$$V_{i+1}(\Delta_{i+1}) < V_i(\Delta_i) \quad \Leftrightarrow \quad V_i(\Delta_i) + V_{i+1}(H_i(t_{i+1})\Delta_i) > 0 \quad \forall \Delta_i \in S^i_k - x^*_i$$

The above inequality is computationally hard, however using the fact that the maps from one switching surface to the next are linear in $S^k_{t_i}$ and that as t_i ranges over $\mathcal{T}_i$, $S^k_{t_i}$ covers every point in S^i_k it is possible to define approximations with a set of LMI (Linear Matrix Inequalities) [31]. We choose to use the conservative condition given by Theorem (2) which is computationally very efficient. Thus equivalently, the limit cycle is globally asymptotically stable if there exist $P_i > 0$ and g_i, $\beta_i = \alpha_i - \alpha_{i+1}$ such that

$$\begin{cases} R_i(t_{i+1}) = P_i - H_i^T(t_{i+1})P_{i+1}H_i(t_{i+1}) - 2(g_i - H_i^T(t_{i+1})g_{i+1})w_i(t_{i+1}) + w_i^T(t_{i+1})\beta_i w_i(t_{i+1}) \\ R_i(t_{i+1}) > 0 \quad \text{on} \quad S^k_{t_i} - x^*_i \quad \text{for all expected switching times} \quad t_i \in \mathcal{T}_i. \end{cases}$$

Furthermore, parameterising the impact map by a switching time corresponds to defining a linear operator $H : \mathbb{R}^{n-1} \to \mathbb{R}^{n-1}$. In view of that, while Δ_i are vectors in $\mathbb{R}^n$ the impact maps have solutions restricted to the hyperplanes in $\mathbb{R}^{n-1}$. Consequently this allows to define *basis* for the switching surfaces where then each vector $\Delta_i \in S^i_k$ can be expressed as linear combination of the *basis* $\Delta_i = \Pi_i \delta_i$ (with Π_i being the *basis* and $\delta_i \in \mathbb{R}^{n-1}$). An easy choice for the *basis* is the *orthogonal complements* to C_i, i.e $\Pi_i \in C_i^{\perp}$. It then follows that the last LMI condition can be rewritten as

$$\begin{cases} R_i(t_{i+1}) = Q_i - F_i^T(t_{i+1})Q_{i+1}F_i(t_{i+1}) - 2(\rho_i - F_i^T(t_{i+1})\rho_{i+1})\omega_i(t_{i+1}) + \omega_i^T(t_{i+1})\psi_i\omega_i(t_{i+1}) \\ R_i(t_{i+1}) > 0 \quad \text{on} \quad S^k_{t_i} - x^*_i \quad \text{for all expected switching times} \quad t_i \in \mathcal{T}_i, \end{cases} \tag{43}$$

where $Q_i = \Pi_{i+1}^T P_i \Pi_i$, $F_i(t) = \Pi_{i+1}^T H_i(t) \Pi_i$, $\rho_i = \Pi_{i+1}^T g_i \Pi_i$, $\psi_i = \Pi_{i+1}^T \beta_i \Pi_i$ and $\omega_i(t) = \Pi_{i+1}^T w_i(t) \Pi_i$. Since the systems within a single region are linear then simple candidates for the quadratic surface coefficients are $\rho_i = 0$ and $\psi_i = 0$. The final aspect to note about condition (43) is that it defines an infinite set of LMI for all $t_i \in \mathcal{T}_i$. Computationally to overcome this difficulty it is necessary to grid

this set in order to obtain a finite subset of expected switching times $t_i^- = t_i^0 < t_i^1 < \cdots < t_i^j = t_i^+$, for some $j \in \mathbb{N}$. To compute the above conditions we implement a set of MATLAB routines using the IQCβ *toolbox* [32]. The objective being to find $Q_i > 0$ and to confirm that (43) is satisfied for all switching times $[t_i^-, t_i^+]$ by plotting the minimum eigenvalue of (43) on $[t_i^-, t_i^+]$, and thus showing that this is indeed positive definite. We find that the largest switching time sets for which (43) are satisfied were $\mathcal{T}_1$=[5.71e-2, 7e-2], $\mathcal{T}_2$=[1e-2, 2.5e-2], $\mathcal{T}_3$=[2.2e-3, 8.85e-3] and $\mathcal{T}_4$=[1.5e-2, 6.4e-2] which can be confirmed in the following Fig. 8. In particular for the switching times presented in Table 3 we have the following positive definite matrices.

$$\mathbf{Q_1} = \begin{pmatrix} 3.63 & 1.38\text{e-}2 & 0 \\ 1.38\text{-}2 & 8.97\text{e-}1 & 0 \\ 0 & 0 & 2.39\text{e-}1 \end{pmatrix} \quad , \quad \mathbf{Q_2} = \begin{pmatrix} 2.33\text{e-}01 & 0 & 0 \\ 0 & 4.88 & \text{-}2\text{e-}01 \\ 0 & \text{-}2\text{e-}01 & 9.17\text{e-}01 \end{pmatrix}$$

$$\mathbf{Q_3} = \begin{pmatrix} 1.61 & \text{-}1.61\text{e-}02 & 0 \\ \text{-}1.61\text{e-}02 & 3.16\text{e-}01 & 0 \\ 0 & 0 & 2.54\text{e-}02 \end{pmatrix} \quad , \quad \mathbf{Q_4} = \begin{pmatrix} 2.37\text{e-}03 & 0 & 0 \\ 0 & 2.49 & 4.22\text{e-}03 \\ 0 & 4.22\text{e-}03 & 7.75\text{e-}02 \end{pmatrix}.$$

Having found that positive definite matrices exist, satisfying Theorem (2) we have proved that the piecewise linear approximation considered is globally asymptotically stable. Other piecewise approximations could have been used but the approximation we considered is sufficient to prove global stability. Note that global stability can equally be proven for this PLS system with time invariant inputs by applying the same procedure. For this case in particular a more straightforward approach could be used by first applying a coordinate transformation. Having proven global stability of the limit cycle for a subset of the control parameters, it leaves us with the question on how to get a suitable approximation for the nonlinear functions that permits an analysis of the system for the complete parameter range. Clearly, consideration of a higher order piecewise approximations will increase the accuracy of the system, whilst also increasing the computational complexity of the LMIs, which does not seem to be necessary. Naturally an interesting extension of this work would be to determine the simplest partition of the state space (V_s, V_r) that permits the global analysis of the limit cycle for the whole parameter domain.

6 Conclusions and future work

In this paper, we have considered theoretical and computational insights into the dynamics of an RKII set, which is to our knowledge the first such rigourous presentation of the existence and stability of limit cycles in a model of this type. Using normal forms and the theory of centre manifolds we were able to extract the coefficients of the Hopf bifurcations, confirming their supercritical nature which we observed computationally in section 3.1. Subsequently we considered a suitable piecewise linear reduction of the RKII set, demonstrating global stability of the limit cycle in this case. A drawback of the chosen approximation is that it was only valid on a subset of the total parameter space and consequently future work should consider a more systematic partitioning of the sigmoidal function, that is, a greater number of partitions of the state space, which would envisage having the effect of smoothing out the observed limit cycle. However, numerical simulations demonstrated that the limit cycle lived in a very restricted region of the state space. Therefore, increasing the number of partitions arbitrarily may well introduce redundancy into the problem whilst increasing the complexity of the calculations. With regards to the biological relevance, the sigmoidal curve originally considered in the model was fitted from clinical data, thus the curve may be considered as some approximation that is representative of the data. On the other hand, sigmoidal curves (Frequency-Current or F-I curves) based on single neuron models, for example Hodgkin-Huxley, are obtained by averaging over piecewise smooth firing rate functions for each individual neuron, an approach commonly used to derive firing-rate/neural field models. Noise in the system smoothes out the average F-I curve and makes the final positioning of the curve somewhat arbitrary and therefore the particular partitioning is only an approximation. Determining the particular partitioning was done by numerically observing that the limit cycle lived in a restricted region of the state space for the parameter values considered and selecting an approximation that partitioned this region. Future work will be to consider extensions of the piecewise linear approximations to enable study of a wider region of parameter space, as well as developing techniques for studying coupled RKII sets and synchronization between them. Further extensions to this work will also consider robustness and performance to guarantee finite gain $\mathcal{L}_2$ stability, in particular for RKII set with periodic inputs. This will allow to complement the results obtained in [12, 11] to better understand the genesis of epilepsy. Finally the strength of this new methodology suggests the potential towards understanding the total Ki set hierarchy and giving hope in understanding human EEG and brain dynamics at the meso and macroscopic levels.

7 Acknowledgments

The authors would like to thank Mark Groves for some very helpful discussions concerning the calculation of the normal forms and to thank the referees for their perceptive comments on a previous draft of the paper. Financial support from the Leverhulme Trust Theoretical Neuroscience Network and the EPSRC via grant EP/D068436/01 is also acknowledged.

References

[1] W. J. Freeman *Mass Action In The Nervous System* (Academic Press, New York) (1975).

[2] R. Kozma and W. J. Freeman, Int. J. Bifurcation & Chaos. **11**(6), 2307-2322 (2001).

[3] H. R. Wilson and J. D. Cowan, Biophys. J. **12**, 1-12, (1972)

[4] J. Principe, V. Tavares, J. Harris and W. J. Freeman, Proc. IEEE. Vol **89**, No 7, 569-571 (2001).

[5] Heng-Jen Chang and W. J. Freeman, Neural Networks. Vol **9**, No 1, 1-14 (1996).

[6] R. Kozma, IEEE Trans. on Neural Networks Vol **16**, No 3, (2005).

[7] R. Ilin and R. Kozma, Phys. Lett. A **360**, 66–83 (2006).

[8] Dongming Xu and J. C. Principe, IEEE Trans. Neural Net. **15** 1053 (2004).

[9] A. Destexhe and T. J. Sejnowski *Thalamocortical Assemblies* (OUP) (2001); A. Destexhe and T. J. Sejnowski, Physiol. Rev. **83**, 1401 (2003).

[10] F. H. Lopes da Silva, A. Hoecks, H. Smits and L. H. Zetterberg, Kybernetik **15**, 27–37 (1974).

[11] M. Breakspear, J. A. Roberts, J. R. Terry, S. Rodrigues, N. Mahant and P. A. Robinson, Cereb. Cortex **16**, 1296–1313 (2006).

[12] S. Rodrigues, J. R. Terry and M. Breakspear, Phys. Lett. A **355**, 352–357 (2006).

[13] W. R. Garnett in J. T. Dipiro et al., (Ed) Pharmacotherapy 1179-1209 (1997).

[14] S. Rodrigues, A. V. Chizhov and J. R. Terry. Mappings between a macroscopic neural mass model and a reduced conductance-based model (submitted) Preprint available at:

`http://www.enm.bris.ac.uk/staff/jrt/publications.html)`

[15] B. Ermentrout *Simulating, Analyzing, and Animating Dynamical Systems. A Guide to XPPAUT* SIAM (2002).

[16] J. Goncalves, A. Megretski and M. Dahleh, IEEE Trans. Automatic Control **48**, 2089–2106 (2003).

[17] P. A. Robinson, C. J. Rennie and J. J. Wright, Phys. Rev. E **56**, 826 (1997); P. A. Robinson, C. J. Rennie, J. J. Wright and P. D. Bourke, Phys. Rev. E **58**, 3557 (1998); C. J. Rennie, P. A. Robinson and J. J. Wright, Phys. Rev. E **59**, 3320 (1999); C. J. Rennie, P. A. Robinson and J. J. Wright, J. Theor. Biol. **205**, 17 (2000).

[18] P. A. Robinson, C. J. Rennie and D. L. Rowe, Phys. Rev. E **65**, 041924 (2002).

[19] F. H. Lopes da Silva, A. Hoecks, H. Smits, L. H. Zetterberg, Kybernetik **15**, 27–37 (1974).

[20] V. K. Jirsa and H. Haken, Phys. Rev. Lett. **77**, 960–963 (1996).

[21] Y. Kuznetsov, L. Kuznetsov and J. Marsden *Elements of Applied Bifurcation theory* (Springer-Verlag, New York) (1998).

[22] F. R. Gantmacher *Application Of The Theory Of Matrices* (Interscience Pub. New York) (1959).

[23] A.I. Mees and L. O. Chua., The Hopf Bifurcation theorem and its applications to nonlinear oscillations in circuits and systems., IEEE Trans. on Circuits and Systems CAS-26 **4** 235-254 (1979).

[24] A. Mees, *Dynamics of feedback systems* (Wiley-Interscience) (1981).

[25] G. Iooss and M. Adelmeyer *Topics in Bifurcation Theory and Applications, advanced series in nonlinear dynamics Vol. 3* (World Scientific, Singapore) (1992).

[26] C. Elphick, E. Tirapegui, M. E. Brachet, P. Coullet and G. Iooss., A Simple Global Characterization For Normal Forms of Singular Vector Fields., Physica 29D, 95-127 (1987).

[27] J. Gickenheimer and P. Holmes *Nonlinear Oscillations, Dynamical Systems and Bifurcation of Vector Fields* Applied Mathematical Science Vol. 41 (Springer, New York) (1983).

[28] J. Imura and A. van der Schaft, IEEE Tans. Automatic Control **45**(9), 1600–1619, Sept (2000).

[29] S. Pettersson and B. Lennartson. An LMI approach for stability analysis of nonlinear systems. EEC, Brussels, Belgium July 1997.

[30] A Hassibi and S. Boyd. Quadratic stabilization and control of piecewise linear systems. ACC, Philadelphia, Pennsylvania, june 1998.

[31] Stephan Boyd, Laurent El Chaoui, Eric Feron and Venkataramanan Balakrishnan *Linear Matrix Inequalities in System and Control Theory* SIAM. ISBN: 0-89871-334-X (1994);

[32] U. Jönsson, C. Kao, A. Megretski, A. Rantzer. (The latest version of the code and manual can be found in

`http://www.ee.unimelb.edu.au/staff/cykao/`)

A

For completeness we provide here additional material relating to the calculation of the normal forms:

A.1 Derivation of the Homological Equation

The normal form/centre manifold methodology introduced by Iooss and Adelmeyer [25] is based on the homological operator. The theory states that the transformation of some vector field to a normal form is possible by the following near identity coordinate transformation $\hat{x} = z + h(z, \hat{\nu})$, where $\hat{x} = (z, y) \in \mathbb{R}^n$ with z a vector on the centre manifold (i.e from equation (17) $z = Ze_0 + \bar{Z}\bar{e_0}$), y a vector on the hyperbolic space and $\hat{\nu} \in \mathbb{R}^n$ the control parameters. To illustrate this, consider the following vector field

$$\dot{\hat{x}} = J\hat{x} + N(x, \hat{\nu}), \tag{44}$$

where J is the linear operator (note that Iooss and Adelmeyer consider the Jacobian) and $N \in C^k(\mathbb{R}^n \times \mathbb{R}^m; \mathbb{R}^n)$ contain the nonlinear terms. The objective is to transform (44) to a normal form on the centre space having the following structure:

$$\dot{z} = Jz + G(z, \hat{\nu}), \tag{45}$$

where $G \in C^k(\mathbb{R}^n \times \mathbb{R}^m; \mathbb{R}^n)$. First, apply the derivative operator to the near identity transformation which gives rise to:

$$\dot{\hat{x}} = \dot{z} + D_z[h(z, \hat{\nu})](\dot{z}). \tag{46}$$

Applying (44) to the above equation (46) results in

$$\dot{z} + D_1[h(z, \hat{\nu})](\dot{z}) = J\hat{x} + N(\hat{x}, \hat{\nu}). \tag{47}$$

Again, introducing the identity transformation into the above equation (46) generates

$$\dot{z} + D_1[h(z, \hat{\nu})](\dot{z}) = Jz + Jh(z, \hat{\nu}) + N(z + h(z, \hat{\nu}), \hat{\nu}). \tag{48}$$

Finally applying (45) to the previous derivation (48) and rearranging terms we obtain the homological operator:

$$Jh(z, \hat{\nu}) - D_z[h(z, \hat{\nu})](Jz) = G(z, \hat{\nu}) - N(z + h(z, \hat{\nu}), \hat{\nu}) + D_z[h(z, \hat{\nu})](G(z, \hat{\nu})).$$

A.2 Derivation of the $\mathcal{O}(1)$ normal form coefficients

The terms that depend linearly on the parameters and coordinates give rise to a homological operator with the following form:

$$Jh_1^1(z,\hat{\nu}) - D_z[h_1^1(z,\hat{\nu})](Jz) = G_1^1(z,\hat{\nu}) - N_1^1(z\hat{\nu}).$$

Since $z = Ze_0 + \bar{Z}\bar{e_0}$ and in our case the control parameters are $\hat{\nu} = (\hat{\nu_{sr}}, \hat{\nu_{rs}})$ then we have the following expansion for h_1^1

$$h_1^1 = h_{1,0}^{1,0}\nu_{sr}Ze_0 + h_{1,0}^{0,1}\nu_{rs}Ze_0 + h_{0,1}^{1,0}\nu_{sr}\bar{Z}\bar{e_0} + h_{0,1}^{0,1}\nu_{rs}\bar{Z}\bar{e_0}. \tag{49}$$

Applying the linear operator J to the above equation (49) results in

$$Jh_1^1 = Jh_{1,0}^{1,0}\hat{\nu_{sr}}Ze_0 + Jh_{1,0}^{0,1}\hat{\nu_{rs}}Ze_0 + Jh_{0,1}^{1,0}\hat{\nu_{sr}}\bar{Z}\bar{e_0} + Jh_{0,1}^{0,1}\hat{\nu_{rs}}\bar{Z}\bar{e_0}. \tag{50}$$

Also apply the multivariate derivative operator D_z to equation (49) to obtain

$$\begin{cases} D_Z[h_2^0(z,\hat{\nu})] = h_{1,0}^{1,0}\hat{\nu_{sr}}e_0 + h_{1,0}^{0,1}\hat{\nu_{rs}}e_0 \\ D_{\bar{Z}}[h_2^0(z,\hat{\nu})] = h_{0,1}^{1,0}\hat{\nu_{sr}}\bar{e_0} + h_{0,1}^{0,1}\hat{\nu_{rs}}\bar{e_0} \end{cases}. \tag{51}$$

The term Jz in the homological equation equates to:

$$\begin{aligned} Jz &= J(Ze_0 + \bar{Z}\bar{e_0}) \\ &\Leftrightarrow \quad ZJ(e_0) + \bar{Z}J(\bar{e_0}) \\ &\Leftrightarrow \quad i\sqrt{\alpha\beta}Ze_0 - i\sqrt{\alpha\beta}\bar{Z}\bar{e_0}. \end{aligned} \tag{52}$$

The expansion of the polynomial G_1^1 has the following form

$$G_1^1 = g_{1,0}^{1,0}\hat{\nu_{sr}}Ze_0 + g_{1,0}^{0,1}\hat{\nu_{rs}}Ze_0 + g_{0,1}^{1,0}\hat{\nu_{sr}}\bar{Z}\bar{e_0} + g_{0,1}^{0,1}\hat{\nu_{rs}}\bar{Z}\bar{e_0} \tag{53}$$

and the nonlinear term N_1^1 is the following

$$N_1^1 = \hat{\nu_{sr}}ZN_1^{0,1}(e_0) + \hat{\nu_{rs}}N_1^{0,1}\bar{Z}(\bar{e_0}). \tag{54}$$

Finally substituting equations (50),(51),(52),(53) and (54) into the homological operator and then equating terms of the same order gives rise to the following four equations:

$$\begin{cases} (J - i\sqrt{\alpha\beta}I)h_{1,0}^{1,0} = g_{1,0}^{1,0}e_0 - N_1^{1,0}(e_0), \\ (J - i\sqrt{\alpha\beta}I)h_{1,0}^{0,1} = g_{1,0}^{0,1}e_0 - N_1^{0,1}(e_0), \\ g_{0,1}^{1,0} = \bar{g}_{1,0}^{1,0}, \\ g_{1,0}^{0,1} = \bar{g}_{0,1}^{0,1}. \end{cases} \tag{55}$$

Here we only consider $g_{1,0}^{1,0}$ and $g_{0,1}^{1,0}$ and to evaluate these coefficients we apply to the individual terms of the first two equations of (55) the inner product with the adjoint dual basis of e_0 and here we denote it as $\bar{f}_0$. Hence we obtain the following:

$$\begin{cases} g_{1,0}^{1,0} < e_0, \bar{f}_0 >=< N_1^{1,0}(e_0), \bar{f}_0 >, \\ g_{1,0}^{0,1} < e_0, \bar{f}_0 >=< N_1^{0,1}(e_0), \bar{f}_0 >, \end{cases} \tag{56}$$

where the operator $< ., . >$ denotes the inner product of two vectors and $< a, b >= a^* b$, where $a, b \in \mathbb{C}$ and a^* is the complex conjugate transpose of vector a and $\bar{f}_0$ is given by equation (27) (refer to the main text), thus

$$< e_0, \bar{f}_0 >= \alpha\beta[2(\alpha+\beta) - (\alpha\beta)] + i(\alpha+\beta)[\sqrt{\alpha\beta}(\alpha+\beta) + \alpha\beta] \tag{57}$$

and

$$N_1^{1,0}(e_0) = \begin{pmatrix} 0 \\ -\alpha\beta\frac{\partial\varsigma[V_r^\star]}{\partial\widehat{V_r}} i\sqrt{\alpha\beta}(\alpha+\beta)\hat{\nu_{sr}} \\ 0 \\ 0 \end{pmatrix} \quad , \quad N_1^{0,1}(e_0) = \begin{pmatrix} 0 \\ 0 \\ 0 \\ -(\alpha\beta)^2\nu_{sr}^* \frac{\partial\varsigma[V_s^\star]}{\partial\widehat{V_s}} \frac{\partial\varsigma[V_r^\star]}{\partial\widehat{V_r}} \hat{\nu_{rs}}. \end{pmatrix}$$

A.3 Derivation of the $\mathcal{O}(2)$ normal form coefficients

From the order 2 homological equation we may extract the coefficients h_0^2. The equation is written in following form

$$Jh_2^0(z) - D_z[h_2^0(z)](Jz) = -N_2^0(z, z)$$

Using the same steps as applied to the order one coefficients and by first performing the Taylor expansion for $h(z)$ of order 2 in z and no dependence on parameters we get

$$h_2^0 = h_{2,0}^0 Z^2 + h_{1,1}^0 Z\bar{Z} + h_{0,1}^0 \bar{Z}^2. \tag{58}$$

Applying the linear operator J to equation (58) we get

$$Jh_2^0 = Jh_{2,0}^0 Z^2 + Jh_{1,1}^0 Z\bar{Z} + Jh_{0,1}^0 \bar{Z}^2. \tag{59}$$

Also we apply the multivariate derivative operator D_z to equation (58) to obtain

$$\begin{cases} D_Z[h_2^0(z)] = 2h_{2,0}^0 Z + h_{1,1}^0 \bar{Z} \\ D_{\bar{Z}}[h_2^0(z)] = h_{1,1}^0 Z + 2h_{0,2}^0 \bar{Z} \end{cases} . \tag{60}$$

Since $Jz = [i\sqrt{\alpha\beta}Z, -i\sqrt{\alpha\beta}]^T$ and then by combining with (60) results in the following:

$$D_z[h_2^0(z)](Jz) = 2h_{2,0}^0 i\sqrt{\alpha\beta}Z^2 - 2h_{0,2}^0 i\sqrt{\alpha\beta}\bar{Z}^2. \tag{61}$$

For the nonlinear term N_2^0, we use the bilinear property of the Taylor expansion for second order terms, which then N_2^0 equates to:

$$N_2^0(z,z) = N_2^0(Ze_0 + \bar{Z}\bar{e_0}, Ze_0 + \bar{Z}\bar{e_0}) \Leftrightarrow Z^2N(e_0,e_0) + 2Z\bar{Z}N(e_0,\bar{e_0}) + \bar{Z}^2N(\bar{e_0},\bar{e_0}). \tag{62}$$

Substituting (52), (58), (61) and (62) back into the homological equation and grouping terms of the same order we get:

$$\begin{cases} (J - 2i\sqrt{\alpha\beta}I)h_{2,0}^0 = -N_2(e_0,e_0) \\ Jh_{1,1}^0 = -N_2(e_0,\bar{e_0}) \\ (J + 2i\sqrt{\alpha\beta}I)h_{2,0}^{\bar{0}} = -N_2(\bar{e_0},e_0) \end{cases}. \tag{63}$$

Note that the eigenvalues of J include $\pm i\sqrt{\alpha\beta}$, so the operator $(J - \eta I)$ is invertible for $\eta \neq \pm i\sqrt{\alpha\beta}$, thus allowing to determine the coefficients $h_{2,0}^0$,$h_{2,0}^{\bar{0}}$ and $h_{1,1}^0$. Where the inverse of the linear operator J at the bifurcation point is given by

$$J^{-1} = \begin{pmatrix} -\frac{\alpha+\beta}{((\alpha+\beta)^2+\alpha\beta)} & -\frac{1}{((\alpha+\beta)^2+\alpha\beta)} & -\frac{\nu_{sr}(\alpha+\beta)\frac{\partial\varsigma[V_r^\star]}{\partial\widehat{V_r}}}{((\alpha+\beta)^2+\alpha\beta)} & -\frac{\nu_{sr}\frac{\partial\varsigma[V_r^\star]}{\partial\widehat{V_r}}}{((\alpha+\beta)^2+\alpha\beta)} \\ 1 & 0 & 0 & 0 \\ -\frac{\nu_{rs}(\alpha+\beta)\frac{\partial\varsigma[V_s^\star]}{\partial\widehat{V_s}}}{((\alpha+\beta)^2+\alpha\beta)} & -\frac{\nu_{rs}\frac{\partial\varsigma[V_s^\star]}{\partial\widehat{V_s}}}{((\alpha+\beta)^2+\alpha\beta)} & -\frac{\alpha+\beta}{((\alpha+\beta)^2+\alpha\beta)} & -\frac{1}{((\alpha+\beta)^2+\alpha\beta)} \\ 0 & 0 & 1 & 0 \end{pmatrix}, \tag{64}$$

and also at the Hopf bifurcation point we have

$$(J - 2i\sqrt{\alpha\beta})^{-1}_{\text{Column 1}} = \frac{1}{det(J - 2i\sqrt{\alpha\beta})} \begin{pmatrix} -7\alpha\beta(\alpha+\beta) + 2i\sqrt{\alpha\beta}((\alpha+\beta)^2 - 3\alpha\beta) \\ \alpha\beta(-2i\sqrt{\alpha\beta}(\alpha+\beta) - (\alpha+\beta)^2 + 3\alpha\beta) \\ \alpha\beta\nu_{rs}\frac{\partial\varsigma[V_s^\star]}{\partial\widehat{V_s}}(\alpha+\beta+2i\sqrt{\alpha\beta}) \\ \alpha\beta\nu_{rs}\frac{\partial\varsigma[V_s^\star]}{\partial\widehat{V_s}}(-4\alpha\beta + 2i\sqrt{\alpha\beta}(\alpha+\beta)) \end{pmatrix}, \tag{65}$$

$$(J - 2i\sqrt{\alpha\beta})^{-1}_{\text{Column 2}} = \frac{1}{det(J - 2i\sqrt{\alpha\beta})} \begin{pmatrix} -3\alpha\beta + 2i\sqrt{\alpha\beta}(\alpha+\beta)) \\ -\alpha\beta(4(\alpha+\beta) + 6i\sqrt{\alpha\beta}) \\ \alpha\beta\nu_{rs}\frac{\partial\varsigma[V_s^\star]}{\partial\widehat{V_s}} \\ 2i\sqrt{\alpha\beta}\nu_{rs}\frac{\partial\varsigma[V_s^\star]}{\partial\widehat{V_s}} \end{pmatrix}, \tag{66}$$

$$(J-2i\sqrt{\alpha\beta})^{-1}_{\text{Column 3}} = \frac{1}{det(J-2i\sqrt{\alpha\beta})}\begin{pmatrix} \alpha\beta\nu_{sr}\frac{\partial\varsigma[V_r^\star]}{\partial\widehat{V_r}}(\alpha+\beta+2i\sqrt{\alpha\beta}) \\ \alpha\beta\nu_{sr}\frac{\partial\varsigma[V_r^\star]}{\partial\widehat{V_r}}(-4\alpha\beta+2i\sqrt{\alpha\beta}(\alpha+\beta)) \\ -7\alpha\beta(\alpha+\beta)+2i\sqrt{\alpha\beta}((\alpha^2+\beta^2)-\alpha\beta) \\ \alpha\beta(3\alpha\beta-(\alpha+\beta)^2-2i\sqrt{\alpha\beta}(\alpha+\beta)) \end{pmatrix}, \tag{67}$$

$$(J-2i\sqrt{\alpha\beta})^{-1}_{\text{Column 4}} = \frac{1}{det(J-2i\sqrt{\alpha\beta})}\begin{pmatrix} \alpha\beta\nu_{sr}\frac{\partial\varsigma[V_r^\star]}{\partial\widehat{V_r}} \\ \alpha\beta\nu_{sr}\frac{\partial\varsigma[V_r^\star]}{\partial\widehat{V_r}}2i\sqrt{\alpha\beta} \\ -3\alpha\beta+2i\sqrt{\alpha\beta}(\alpha+\beta) \\ -2\alpha\beta(2(\alpha+\beta)+3i\sqrt{\alpha\beta}) \end{pmatrix}, \tag{68}$$

where $\det(J-2i\sqrt{\alpha\beta}) = 3\alpha\beta(((\alpha^2+\beta^2)+\alpha\beta)+4i\sqrt{\alpha\beta}(\alpha+\beta))$.

Furthemore we have the following bilinear terms

$$N_2^0(e_0,e_0) = \frac{1}{2!}\begin{pmatrix} 0 \\ -(\alpha\beta)^2(\alpha+\beta)\nu_{sr}^*\frac{\partial^2\varsigma[V_r^\star]}{\partial\widehat{V_r}^2} \\ 0 \\ (\alpha\beta)^3\nu_{rs}^*(\nu_{sr}^*)^2\frac{\partial^2\varsigma[V_s^\star]}{\partial\widehat{V_s}^2}(\frac{\partial\varsigma[V_r^\star]}{\partial\widehat{V_r}})^2 \end{pmatrix}, \tag{69}$$

$$N_2^0(e_0,\bar{e_0}) = \frac{1}{2!}\begin{pmatrix} 0 \\ (\alpha\beta)^2(\alpha+\beta)^2\nu_{sr}^*\frac{\partial^2\varsigma[V_r^\star]}{\partial\widehat{V_r}^2} \\ 0 \\ (\alpha\beta)^3\nu_{rs}^*(\nu_{sr}^*)^2\frac{\partial^2\varsigma[V_s^\star]}{\partial\widehat{V_s}^2}(\frac{\partial\varsigma[V_r^\star]}{\partial\widehat{V_r}})^2 \end{pmatrix}, \tag{70}$$

A.4 Derivation of the $\mathcal{O}(3)$ normal form coefficients

From the order 3 homological equation, we may extract the coefficients that are cubic in the coordinates of the centre space and independent of the control parameters, that is, here $Z\mathcal{O}(|Z|^2)$. The operator takes the following form:

$$Jh_3^0(z) - D_z[h_3^0(z)](Jz) = G_3^0 - 2N_2^0(z,h_2^0(z)) - N_3(z,z,z). \tag{71}$$

The third order Taylor expansion of $h(z)$ gives the following:

$$h_3^0 = h_{3,0}^0Z^3 + h_{2,1}^0Z^2\bar{Z} + h_{1,2}^0Z\bar{Z}^2 + h_{0,3}^0\bar{Z}^3. \tag{72}$$

In same way as for order one and two coefficients, we apply the linear operator J to equation (72). Also, applying the differential operator D_z to (72) we obtain

$$\begin{cases} D_Z[h^0_3(z)] = 3h^0_{3,0}Z^2 + 2h^0_{2,1}Z\bar{Z} + h^0_{1,2}\bar{Z}^2 \\ D_{\bar{Z}}[h^0_3(z)] = h^0_{2,1}Z^2 + 2h^0_{1,2}Z\bar{Z} + 3h^0_{0,3}\bar{Z}^2 \end{cases}. \tag{73}$$

Then by combining (73) and (52) this gives rise to

$$D_z[h^0_3(z)](Jz) = i\sqrt{\alpha\beta}(3h^0_{3,0}Z^3 + h^0_{2,1}Z^2\bar{Z} - h^0_{1,2}Z\bar{Z}^2 - 3h^0_{0,3}\bar{Z}^3). \tag{74}$$

In this case we have the nonlinear term N^0_2 and its derivation is as follows:

$$\begin{aligned} N^0_2(z, h^0_2(z)) &= N^0_2(Ze_0 + \bar{Z}\bar{e_0}, h^0_{2,0}Z^2 + h^0_{1,1}Z\bar{Z} + h^0_{0,2}\bar{Z}^2) \\ &\Leftrightarrow N^0_2(e_0, h^0_{2,0})Z^3 + N^0_2(e_0, h^0_{1,1})Z^2\bar{Z} + N_2(e_0, h^0_{0,2})Z\bar{Z}^2 \\ &+ N^0_2(\bar{e_0}, h^0_{2,0})\bar{Z}Z^2 + N^0_2(\bar{e_0}, h^0_{1,1})Z\bar{Z}^2 + N_2(\bar{e_0}, h^0_{0,2})\bar{Z}^3. \end{aligned} \tag{75}$$

Equally for the third order of the same nonlinearity we have:

$$\begin{aligned} N^0_3(z, z, z) &= N^0_3(e_0, e_0, e_0)Z^3 + 3N^0_3(e_0, e_0, \bar{e_0})Z^2\bar{Z} \\ &+ 3N^0_3(e_0, \bar{e_0}, \bar{e_0})Z\bar{Z}^2 + N^0_3(\bar{e_0}, \bar{e_0}, \bar{e_0})\bar{Z}^3. \end{aligned} \tag{76}$$

The expansion for the cubic terms of the normal form G has the following structure:

$$G^0_3 = g^{0,0}_{2,1}Z|Z|^2e_0 + g^{0,0}_{1,2}\bar{Z}|Z|^2\bar{e_0} \tag{77}$$

$$\Leftrightarrow g^{0,0}_{2,1}Z^2\bar{Z}e_0 + g^{0,0}_{1,2}Z\bar{Z}^2\bar{e_0}. \tag{78}$$

Substituting (52), (72), (74), (75), (76) and (78) back into the homological equation of order 3 and grouping terms of the same order we obtain

$$\begin{cases} (L - i3\sqrt{\alpha\beta}I)h^0_{3,0} = -2N^0_2(e_0, h^0_{2,0}) - N^0_3(e_0, e_0, e_0), \\ (L + i3\sqrt{\alpha\beta}I)h^0_{0,3} = -2N^0_2(\bar{e_0}, h^0_{0,2}) - N^0_3(\bar{e_0}, \bar{e_0}, \bar{e_0}), \\ (L - i\sqrt{\alpha\beta}I)h^{0,0}_{2,1} = g^{0,0}_{2,1}e_0 - 2N^0_2(\bar{e_0}, h^{0,0}_{2,0}) - 2N^0_2(e_0, h^{0,0}_{1,1}) - 3N^0_3(e_0, e_0, \bar{e_0}), \\ (L + i\sqrt{\alpha\beta}I)h^0_{1,2} = g^{0,0}_{1,2}\bar{e_0} - 2N^0_2(e_0, h^{0,0}_{0,2}) - 2N^0_2(\bar{e_0}, h^{0,0}_{1,1}) - 3N^0_3(e_0, \bar{e_0}, \bar{e_0}). \end{cases} \tag{79}$$

Here we only evaluate $g^{0,0}_{1,2}$ and $g^{0,0}_{2,1}$. To solve them we can apply to the last two equations of (79) the inner product with the adjoint dual basis of e_0 which we denote as $\bar{f}_0$. Thus we have the following:

$$\begin{cases} g^{0,0}_{2,1} < e_0, \bar{f}_0 >= 2 < N^0_2(\bar{e_0}, h^{0,0}_{2,0}), \bar{f}_0 > +2 < N^0_2(e_0, h^{0,0}_{1,1}), \bar{f}_0 > +3 < N^0_3(e_0, e_0, \bar{e_0}), \bar{f}_0 > \\ g^{0,0}_{1,2} = \bar{g}^{0,0}_{2,1} \end{cases} \tag{80}$$

where $< e_0, \bar{f}_0 >$ is given by equation (57) in section §A.2, and

$$N_2^0(e_0, h_{1,1}^0) = \frac{-(\alpha\beta)^3(\nu_{sr}^*)^2\nu_{rs}^*}{4[(\alpha+\beta)^2+\alpha\beta]}N_{11} \tag{81}$$

$$N_{11} = \begin{pmatrix} 0 \\ i\sqrt{\alpha\beta}(\alpha+\beta)\frac{\partial^2\varsigma[V_r^\star]}{\partial\widehat{V_r}^2}[(\alpha+\beta)^2\frac{\partial\varsigma[V_s^\star]}{\partial\widehat{V_s}}\frac{\partial^2\varsigma[V_r^\star]}{\partial\widehat{V_r}^2} + \alpha\beta\nu_{sr}^*\frac{\partial^2\varsigma[V_s^\star]}{\partial\widehat{V_s}^2}(\frac{\partial\varsigma[V_r^\star]}{\partial\widehat{V_r}})^2)] \\ 0 \\ \alpha\beta\frac{\partial^2\varsigma[V_s^\star]}{\partial\widehat{V_s}^2}\frac{\partial\varsigma[V_r^\star]}{\partial\widehat{V_r}}[(\alpha+\beta)^2\frac{\partial^2\varsigma[V_r^\star]}{\partial\widehat{V_r}^2} + \alpha\beta\nu_{rs}^*(\nu_{sr}^*)^2\frac{\partial^2\varsigma[V_s^\star]}{\partial\widehat{V_s}^2}(\frac{\partial\varsigma[V_r^\star]}{\partial\widehat{V_r}})^3] \end{pmatrix}.$$

Furthermore

$$\begin{aligned} < N_2^0(e_0, h_{1,1}^0), \bar{f}_0 > &= \frac{-(\alpha\beta)^2(\nu_{sr}^*)^2\nu_{rs}^*}{4[(\alpha+\beta)^2+\alpha\beta]}\left(\nu_{rs}^*\frac{\partial\varsigma[V_s^\star]}{\partial\widehat{V_s}}\frac{\partial^2\varsigma[V_r^\star]}{\partial\widehat{V_r}^2}\left[(\alpha+\beta)^2\frac{\partial\varsigma[V_s^\star]}{\partial\widehat{V_s}}\frac{\partial^2\varsigma[V_r^\star]}{\partial\widehat{V_r}^2}\right.\right. \\ &+ \left.(\alpha\beta)\nu_{sr}^*\frac{\partial^2\varsigma[V_s^\star]}{\partial\widehat{V_s}^2}(\frac{\partial\varsigma[V_r^\star]}{\partial\widehat{V_r}})^2)\right] + \frac{\partial^2\varsigma[V_s^\star]}{\partial\widehat{V_s}^2}\frac{\partial\varsigma[V_r^\star]}{\partial\widehat{V_r}}\left[(\alpha+\beta)^2\frac{\partial^2\varsigma[V_r^\star]}{\partial\widehat{V_r}^2}\right. \\ &+ \left.\left.(\alpha\beta)\nu_{rs}(\nu_{sr})^2\frac{\partial^2\varsigma[V_s^\star]}{\partial\widehat{V_s}^2}(\frac{\partial\varsigma[V_r^\star]}{\partial\widehat{V_r}})^3\right]\right). \end{aligned} \tag{82}$$

The next term equates to the following

$$N_2^0(\bar{e_0}, h_{2,0}^0) = -\frac{(\alpha\beta)^4(\nu_{sr}^*)^2\nu_{rs}^*}{4det(J-2i\sqrt{\alpha\beta})}M_{20}, \tag{83}$$

where M_{20} is the subsequent matrix

$$M_{20} = \begin{pmatrix} 0 \\ i\sqrt{\alpha\beta}(\alpha+\beta)\frac{\partial^2\varsigma[V_r^\star]}{\partial\widehat{V_r}^2}[-(\alpha+\beta)^2\frac{\partial\varsigma[V_s^\star]}{\partial\widehat{V_s}}\frac{\partial^2\varsigma[V_r^\star]}{\partial\widehat{V_r}^2} + \nu_{sr}^*\frac{\partial^2\varsigma[V_s^\star]}{\partial\widehat{V_s}^2}(\frac{\partial\varsigma[V_r^\star]}{\partial\widehat{V_r}})^2)(-3\alpha\beta+2i\sqrt{\alpha\beta}(\alpha+\beta))] \\ 0 \\ -\frac{\partial^2\varsigma[V_s^\star]}{\partial\widehat{V_s}^2}\frac{\partial\varsigma[V_r^\star]}{\partial\widehat{V_r}}(-3\alpha\beta+2i\sqrt{\alpha\beta}(\alpha+\beta))[-(\alpha+\beta)^2\frac{\partial^2\varsigma[V_r^\star]}{\partial\widehat{V_r}^2} + (\alpha\beta)^2(\nu_{sr}^*)^2\nu_{rs}^*\frac{\partial^2\varsigma[V_s^\star]}{\partial\widehat{V_s}^2}(\frac{\partial\varsigma[V_r^\star]}{\partial\widehat{V_r}})^3] \end{pmatrix},$$

which then applying the inner product with $\bar{f}_0$ results in

$$\begin{aligned} < N_2^0(\bar{e_0}, h_{2,0}^0), \bar{f}_0 > &= -\frac{(\alpha\beta)^4(\nu_{sr}^*)^2\nu_{rs}^*}{4det(J-2i\sqrt{\alpha\beta})}\left(-(\alpha\beta)\nu_{rs}^*\frac{\partial^2\varsigma[V_r^\star]}{\partial\widehat{V_r}^2}\frac{\partial\varsigma[V_s^\star]}{\partial\widehat{V_s}}\left[(\alpha+\beta)^2\frac{\partial^2\varsigma[V_r^\star]}{\partial\widehat{V_r}^2}\frac{\partial\varsigma[V_s^\star]}{\partial\widehat{V_s}}\right.\right. \\ &+ \left.\nu_{sr}\frac{\partial^2\varsigma[V_s^\star]}{\partial\widehat{V_s}^2}(\frac{\partial\varsigma[V_r^\star]}{\partial\widehat{V_r}})^2[3\alpha\beta+2i\sqrt{\alpha\beta}(\alpha+\beta)]\right] \\ &+ \frac{\partial^2\varsigma[V_s^\star]}{\partial\widehat{V_s}^2}\frac{\partial\varsigma[V_r^\star]}{\partial\widehat{V_r}}(3\alpha\beta+2i\sqrt{\alpha\beta}(\alpha+\beta))\left[-(\alpha+\beta)^2\frac{\partial^2\varsigma[V_r^\star]}{\partial\widehat{V_r}^2}\right. \\ &+ \left.\left.(\alpha\beta)^2(\nu_{sr}^*)^2\nu_{rs}^*\frac{\partial^2\varsigma[V_s^\star]}{\partial\widehat{V_s}^2}(\frac{\partial\varsigma[V_r^\star]}{\partial\widehat{V_r}})^3\right]\right) \end{aligned} \tag{84}$$

For the third order nonlinearities we have

$$N_3^0(e_0,e_0,\bar{e_0}) = -\frac{1}{3!}\begin{pmatrix} 0 \\ i\sqrt{\alpha\beta}(\alpha\beta)^2(\alpha+\beta)^3\nu_{sr}^*\frac{\partial^3\varsigma[V_r^\star]}{\partial\widehat{V_r}^3} \\ 0 \\ (\alpha\beta)^4(\nu_{sr}^*)^3\nu_{rs}^*\frac{\partial^3\varsigma[V_s^\star]}{\partial\widehat{V_s}^3}(\frac{\partial\varsigma[V_r^\star]}{\partial\widehat{V_r}})^3 \end{pmatrix}$$

$$\begin{aligned} < N_3^0(e_0,e_0,\bar{e_0}),\bar{f}_0 > &= -\frac{(\alpha\beta)^3\nu_{sr}^*\nu_{rs}}{3!}\left((\alpha+\beta)^2\frac{\partial\varsigma[V_s^\star]}{\partial\widehat{V}_s}\frac{\partial^3\varsigma[V_r^\star]}{\partial\widehat{V_r}^3}\right. \\ &+ \left.(\nu_{sr})^2(\alpha\beta)\frac{\partial^3\varsigma[V_s^\star]}{\partial\widehat{V}_s^3}(\frac{\partial\varsigma[V_r^\star]}{\partial\widehat{V_r}})^3\right) \end{aligned}$$

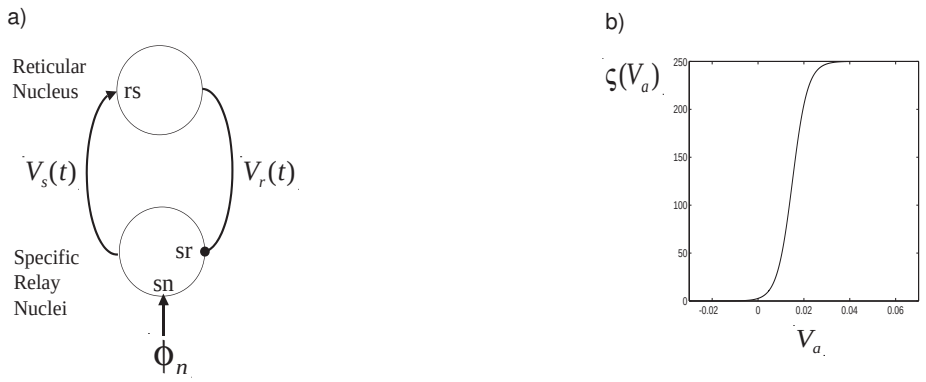

Figure 1: a)Thalamic neuronal population based on Freeman's neural activity mathematical formulation. The model is usually denoted RKII as it is a reduction of the standard KII set, in that it is a special case where the functional topology is such that only an excitatory/inhibitory interaction is considered. The excitatory neuron population is denoted the specific relay while the inhibitory population is termed the reticular. The synaptic strengths are $\nu_{sr} < 0$ and $\nu_{rs} > 0$. The external forcing ϕ_n is an external signal but here we only consider a time invariant signal and where $\nu_{sn} \geq 0$. b) The neurons (inhibitory and excitatory) are coupled by a unipolar sigmoidal, which transforms the neurons transmembrane potential V_a (generally expressed as *wave amplitude*) into firing rate $\varsigma(V_a)$ (termed *pulse density*), i.e voltage-frequency relation. Note the scale of the x-axes and y-axes (-0.03,0) to (0.07, 250). This is related to the averaging performed over a mm^3 of neural tissue, which is a highly nonlinear mechanism.

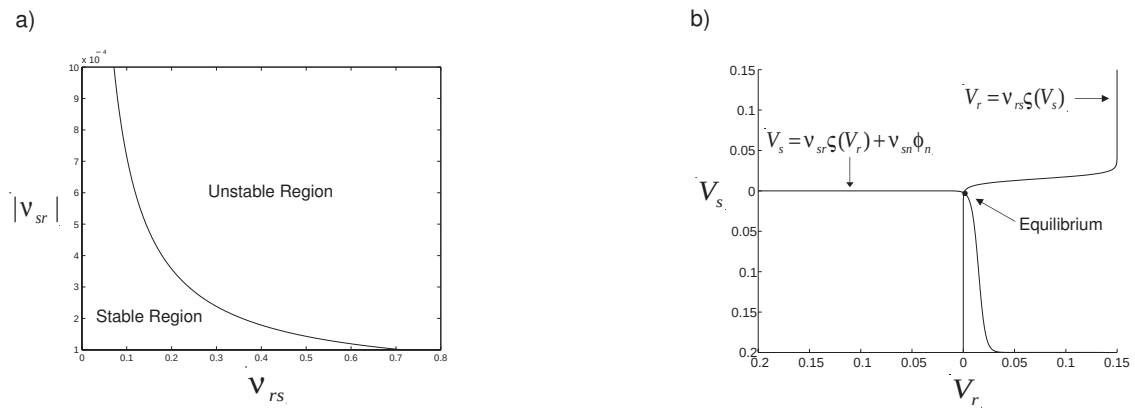

Figure 2: a) Illustrating the stability condition (6) in the parameter space $|\nu_{sr}\nu_{rs}|$. In this case, the values of the fixed point is given by $V_s^* = -0.01222$ and $V_r^* = 0.005962$. The curve is hyperbolic, giving a stable and an unstable region. This transition from stable to unstable defines the branch in parameter space where a supercritical Hopf bifurcation occurs. b) Illustrative example of the nullclines of system (2) in the state space (V_s, V_r). Since the sigmoidal curve is monotonic, there exists a unique equilibrium point for a fixed set of parameters. The equilibrium can either be in the first or fourth quadrant of the state space (V_s, V_r) depending on the level of the strength of external input ν_{sn}.

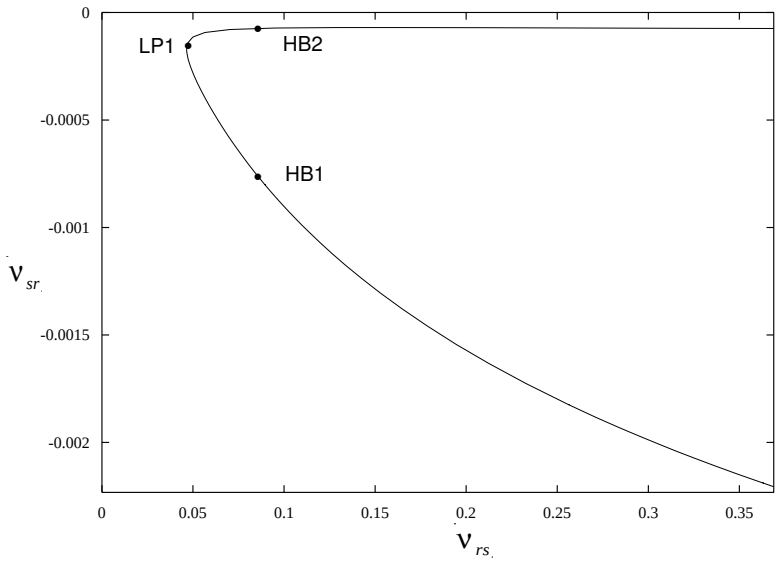

Figure 3: Illustrated is a two parameter branch of Hopf bifurcations in the (ν_{sr}, ν_{rs}) parameter space . A numerical continuation finds extra structure in this parameter space. The lower part of the curve confirms the hyperbolic nature of the (ν_{sr}, ν_{rs}) parameter space given by Eqn (6), however there is additionally a fold point (LP1). From this fold point, two Hopf bifurcations are born, both supercritical (HB1) and (HB2). All values of the special points depicted are given in Table (2).

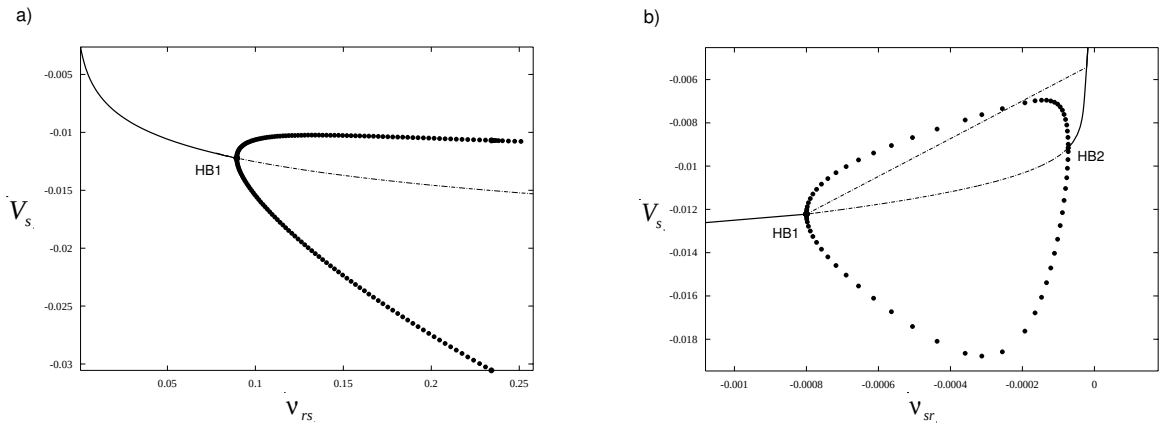

Figure 4: a) Plotted is a bifurcation diagram (V_s,ν_{rs}) for the autonomous case. Commencing from HB1 where $\nu_{sr} = -0.0008$ and varying ν_{rs}, the amplitude of the periodic orbits appearing from HB1 gradually augment to a maximum but never decays. This characteristic can be verified by examining the previous Fig. 3, since it is a parabolic curve, if the system starts from HB1 with ν_{sr} fixed and simultaneously varying ν_{rs} then the system never intersects a section of the (ν_{sr}, ν_{rs}) curve. The labeled points of interest have their actual values laid in table (2). b) Illustrating the bifurcation diagram (V_s,ν_{sr}) where $\nu_{rs} = 0.0894$ (fixed). Starting from HB1 and varying ν_{sr} the amplitude of the Hopf grows to a maximum and then decays until it finds HB2. Note the extra unstable fixed points starting from HB1 and moving up diagonaly until it gains stability. The point where it gains stability is very close to the fold point LP1. This point was numerically unstable and XPP found it difficult to follow the Hopf bifurcation close to LP1. The special points marked in the figures have their corresponding values stored in table (2).

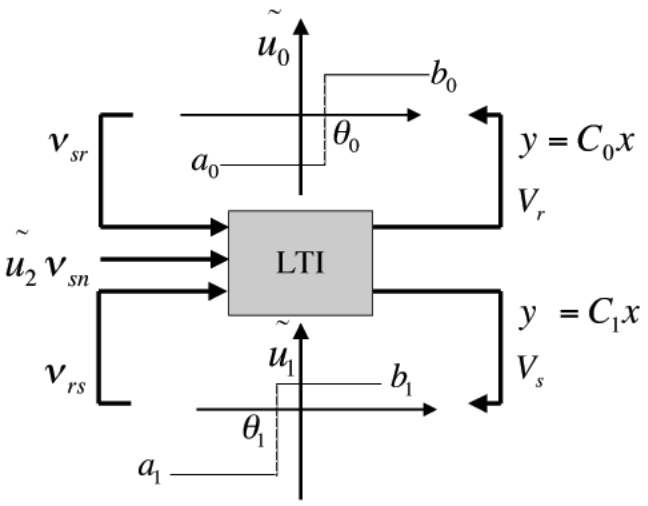

Figure 5: Illustrating the piecewise approximations applied to the original model. The nonlinear terms are approximated and seen as driving terms to the LTI system and since the system also includes a time invariant signal thus three vectors representing inputs to the system are defined $(\tilde{u_0}, \tilde{u_1}, \tilde{u_2})$. Two most relevant hyper-planes are defined as $C_0 x$ and $C_1 x$ for which the systems solutions will intersect them.

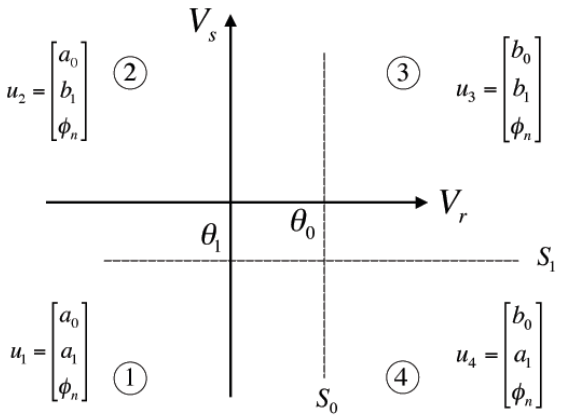

Figure 6: The figure shows the state space (V_s, V_r) and how the hyperplanes situate in this projection space. The hyperplanes are defined as $C_0 x$ and $C_1 x$ which are orthogonal to one another and which are denote as the switching surfaces S_0 and S_1 respectively. Each subspace is defined by an independent LTI flow of the form $\dot{x} = Ax + Bu$, where all the four systems differ in how the vector u is defined. The vectors are defined as $u_i = [\tilde{u_0}, \tilde{u_1}, \tilde{u_2}]^T$, with $i \in \{1, 2, 3, 4\}$. The values assumed by $\tilde{u_0}$ and $\tilde{u_1}$ are related to where System$_i$ situates with respect to the Heaviside function thresholds θ_0 and θ_1 respectively and here $\tilde{u_2} = \phi_n = 1$.

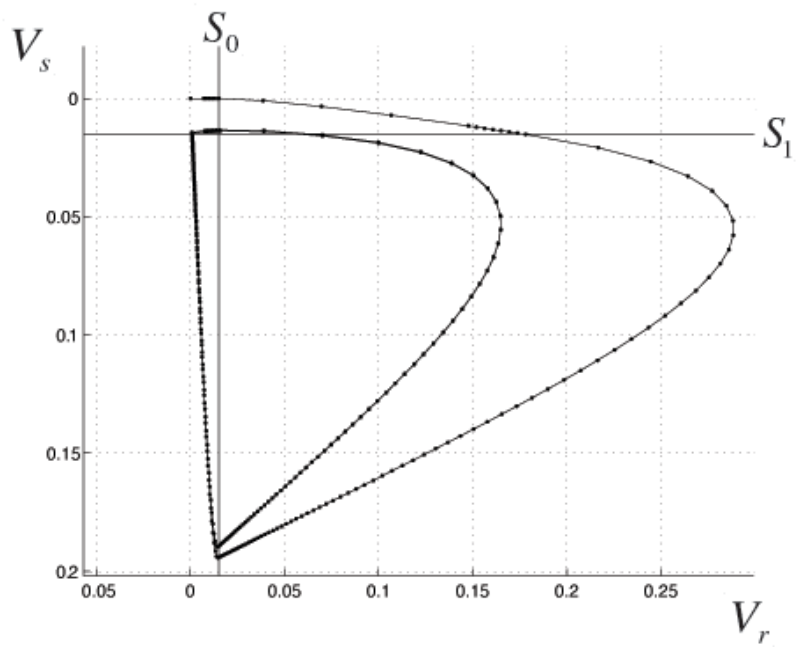

Figure 7: Simulation of the four systems of each partition of the state space and with the initial condition $x_0^* = [0, 0, 0, 0]^T$. The control parameters are set to $\nu_{sr} = -0.008$, $\nu_{rs} = 0.006$ and $\nu_{sn} = 0$ which corresponds to the Hopf bifurction point HB1 (see Table 2). System$_2$ starts running and its trajectory is towards its equilibrium point which lies in the first quadrant and a switch occurs at S_0. in the first quadrant System$_3$ takes over a moves towards its own equilibrium on the fourth quadrant and a second switch occurs at S_1. For the other two final systems (4 and 1) identical scenario occurs, where System$_1$ has its equilibrium on the second quadrant and $System_4$ on the third quadrant. Note that if S_1 was slightly shifted upwards then the limit cycle condition would no longer be satisfied and the limit cycle would vanish. Thus this also explains the generation of the Hopf bifurcation HB1.

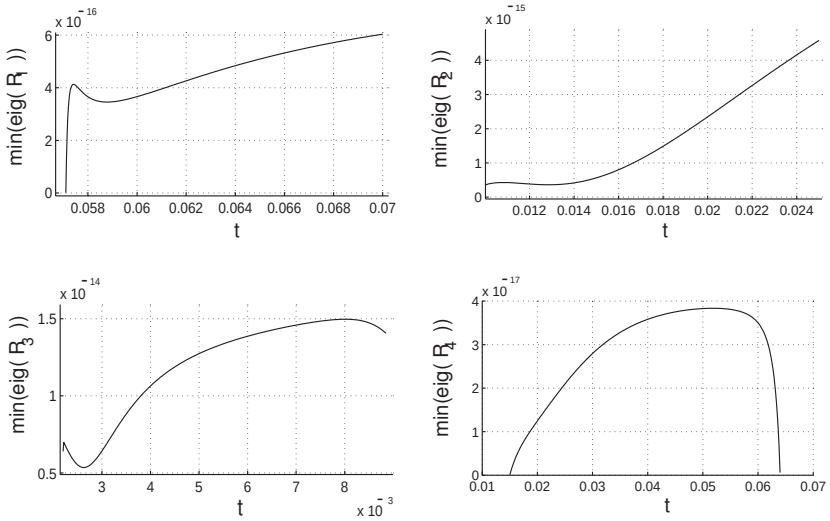

Figure 8: SuLF for all the four impact maps are stable. Each plot shows the minimum eigenvalue of (43) on the respective sets of switching times $\mathcal{T}_i$ for each impact map. The eigenvalues of (43) are always positive for $\mathcal{T}_i$ (feasible) meaning that a positive definite matrix always exists and thus a SuLF for each impact map exists and is stable. In this way it is shown that the limit cycle is globally asymptotically stable.

Quantity	Description	*Values*
θ	Threshold of membrane potential before a cell fires.	0.015 V
σ	Standard deviation of neuron firing probability,versus cell membrane potential.	0.006 V
$Q^{\max}$	Mean maximum firing rate of a cell.	250 s^{-1}
α	Receptor offset time constant (inverse of decay time of potential produced at synapse).	50 s^{-1}
β	Receptor onset time constant (inverse of inverse rise time of potential produced at synapse).	200 s^{-1}
ν_{sn}	Subthalamic signal strength.	20e-4 Vs
ν_{sr}	Coupling strength between *reticular* and *specific relay* neurons.	-8e-4 Vs
ν_{rs}	Coupling strength between *specific relay* and *reticular* neurons.	6e-4 Vs

Table 1: Typical parameter values for the model.

Label	Type	V_s	V_r	ν_{sn}	ν_{sr}	ν_{rs}
LP1	Fold point from which two Hopf are born.	-0.008262	0.01026	0	-0.0001714	0.04654
HB1	Supercritical Hopf.	-0.01222	0.005962	0	-0.0008	0.0894
HB2	Supercritical Hopf.	-0.009158	0.01504	0	$-7.28e-5$	0.0894

Table 2: The relevant critical points.

Switching times	Poincaré surface coordinates
$t_1^* =$ 5.8e-02	$x_1^* =$ [-1.48e-02, 7.41e-01, 8.39e-04, -4.19e-02]^T
$t_2^* =$ 1.6e-02	$x_2^* =$ [-1.38e-02, 6.88e-01, 1.57e-02, 1.87e+01]^T
$t_3^* =$ 3.0e-03	$x_3^* =$ [-1.58e-02, -2.5e+00, 7.01e-02, 3.42e+01]^T
$t_4^* =$ 6.3e-02	$x_4^* =$ [-1.90e-01, -5.15e-01, 1.45e-02, -7.25e-01]^T

Table 3: Switching times and coordinates for all the four systems.